NTNU – Trondheim
Norwegian University of
Science and Technology

Vapor Liquid Equilibrium (VLE) in H2O-Amine-CO2 system

Rafiq Ahmad

Chemical Engineering
Submission date: July 2012
Supervisor: Hallvard Fjøsne Svendsen, IKP
Co-supervisor: Ardi Hartono, IKP

Norwegian University of Science and Technology
Department of Chemical Engineering

Dedicated to my

Beloved parents

and

my lovely wife

Abstract

New experimental data for vapor-liquid equilibrium of CO_2 in aqueous solutions of 3M/26.84% wt, 1M/9% wt and 0.1M/0.89% wt AMP (2-amino-2-methyl-1-propanol) and 1.5M PZ are reported from 313 to 393K. Low pressure/temperature equilibrium apparatus was used to measure the CO_2 partial pressure over loaded AMP solutions while total pressure was measured with high pressure/temperature equilibrium apparatus.

The experiments cover the temperature range of (313K–353K) and CO_2 partial pressure range of (0.0207-18.67KPa) for AMP solutions. The experiments also present total pressure range (222.4-1001.9KPa) and (222.4-973.9KPa) for AMP and PZ systems at temperature range of (353-393K) respectively.

A thermodynamic model representing the AMP system was developed using the e-NRTL framework. The binary interaction parameters (molecule-molecule) for AMP-H_2O system were regressed using binary VLE data and excess enthalpy data from literature in NRTL equation. Then these binary interaction parameters were fixed and regressed the ternary interaction parameters using the VLE data and physical CO_2 solubility data of this work.

The model gives a good representation of experimental binary VLE data and excess enthalpy data with an AARD of 0.01% and 5.9% respectively. The model also gives an excellent agreement for CO_2 partial pressure and total pressure for all AMP concentrations with an AARD of 20.7% and 14.26% while the physical solubility data was predicted with in an AARD of 31.7579%. Further, the model predicts the liquid phase speciation.

Acknowledgement

Alhamdulillah, thesis work in the field of CO_2 absorption is carried out at the department of Chemical Engineering; NTNU Trondheim, Norway has been finished and reported in this master thesis. I would like to express my deepest gratitude to all those who have helped me along the way.

First of all, I would like to thank my supervisor, Professor Hallvard F. Svendsen, for providing me an opportunity to join in the CO_2 group to complete my master degree at the department. I would like to thank him for his supervision with his trustworthy advice and support during my whole research work.

I give special thanks to my co-supervisor Dr. Ardi Hartono for all his guidance from the very first day this work start. His patience, kindness, advice and insights are highly appreciated. He always spared his time for useful discussions especially in modeling and review of my work. He played a vital role in squeezing the best in me. I wish to thank Dr. Inna Kim for her valuable discussion and suggestions.

I also want to thank my best friend Muhammad Usman for his valuable support. I give special thank to my lovely parents for the foundation they laid for my life, their prayers and support are invaluable. I must thank my wife for her support and understanding during this work.

I declare that all this work is independent and according to exam regulations of Norwegian University of Science and Technology.

NTNU, Trondheim

02.07.2012

Author

Table of Contents

Nomenclature

A, *B*,*C*,*D*	Constants [-]
H	Henry's constant [kPa m^3/mol]
K	Equilibrium constant
M	Molarity (mole/liter)
M_s	Solvent molecular weight (g/mole)
N_0	Avogadro's number
P =	Pressure (Pa)
P_s^0	Saturation pressure of solvent s (Pa)
R	Gas Constant (8.314 J/mole.K)
T	Temperature, K
X	Effective mole fraction
e	Electron charge
d	Solvent density (g/cm^3)
G	Gibbs free energy (J)
k	Boltzmann constant
n_t	Total mole number for all species in the system
n_i	Mole number of species *i*
r	Born radius (cm)
v	Molar volume (l/mole)

∇	Partial molar volume (l/mole)
w_s	Weight fraction
x	True liquid-phase mole fraction based on all species: molecular and ionic
y	Vapor-phase mole fraction

Greek Letters

α	Liquid phase loading of CO_2, [mol CO_2 / mol amine]
α	NRTL non-randomness factor
γ	Activity coefficient
ρ	Closest approach parameter of the Pitzer–Debye–Hückel equation
τ	NRTL interaction parameter
ϕ	Fugacity coefficient

SUBSCRIPTS

a, a‘, a‘ ‘	Anion
c, c‘, c‘ ‘	Cation
i, *j*, *k*	Any species
m, m‘	Molecular species
s	Solvent

Abbreviations

AMP	2-amino-2-methyle-1-propanol

PZ	Piperazine
$BaCO_3$	Barium carbonate
$BaCl_2$	Barium chloride
CO_2	Carbon dioxide

List of Figures

List of Tables

Chapter 1

Introduction

1.1 Background

Global climate change, energy efficiency improvements and switching from fossil fuels towards less carbon emissions fuels have become the vital issues regarding energy and environment. Human beings are said to contribute more to global climate change through burning of fossil fuels and industrial processes by emitting greenhouse gas emissions. These emissions trap heat in them and are responsible for global rise in temperature. The most critical GHG emissions is carbon dioxide and it has accounted for 82% of total US GHG emissions in terms of global climate change and 96% of these CO_2 emissions are resulted from burning of fossil fuels (EPA, 2002).

The formula below can be used for understanding the main drivers for CO_2 emissions: (Soren Anderson and Richard Newell., 2003)

$$CO_2 \text{ emissions} = GDP \times \frac{\text{Energy consumption}}{\text{Unit GDP}} \times \frac{CO_2 \text{ emissions}}{\text{Unit energy consumption}}$$

GDP = Gross domestic Product, measure of the size of economy

Fossil fuels will provide about 80% of total world energy requirements for the coming decades. Coal and natural gas are the main contributors to fulfill the energy demand by 38% and 30% respectively by 2030 (IEA, 2004a). Coal accounted 24%, natural gas 21%, nuclear 5%, hydropower 6% and renewables 10% for the primary energy demands (BP, 2005). Power generation is the largest source of CO_2 emissions (IEA GHG, 2002b).

Flue and stack gases from power sector are at atmospheric pressure with varying concentrations of CO_2. In addition to this, other stationary sources of CO_2 emissions are from natural gas sweetening, hydrogen production for ammonia and ethylene oxide, oil refineries, iron and steel production facilities, cement, transportation sector and limestone manufacturing plants.

1.2 Carbon capture and storage

Analysts and policymakers have now realized to develop end-of-pipe technologies for utilization of fossil fuel energy sources and reducing CO_2 emissions. These technologies are known as carbon capture and storage technologies. Carbon capture and storage (CCS) is well-thought-out to be technically feasible at commercial scale using a range of technologies. The major components of a CCS value chain include separation and compression to supercritical state, transport and storage including measurement, monitoring and verification of safe operations.

1.2.1 CO_2 capture technologies

There are three methods to capture CO_2 from the point sources.

- Pre-Combustion CO_2 capture
- Post-Combustion CO_2 capture
- Oxy-fuel Combustion

The operating principles of these methods have been depicted in the fig.1.1. These methods are explained one by one as under.

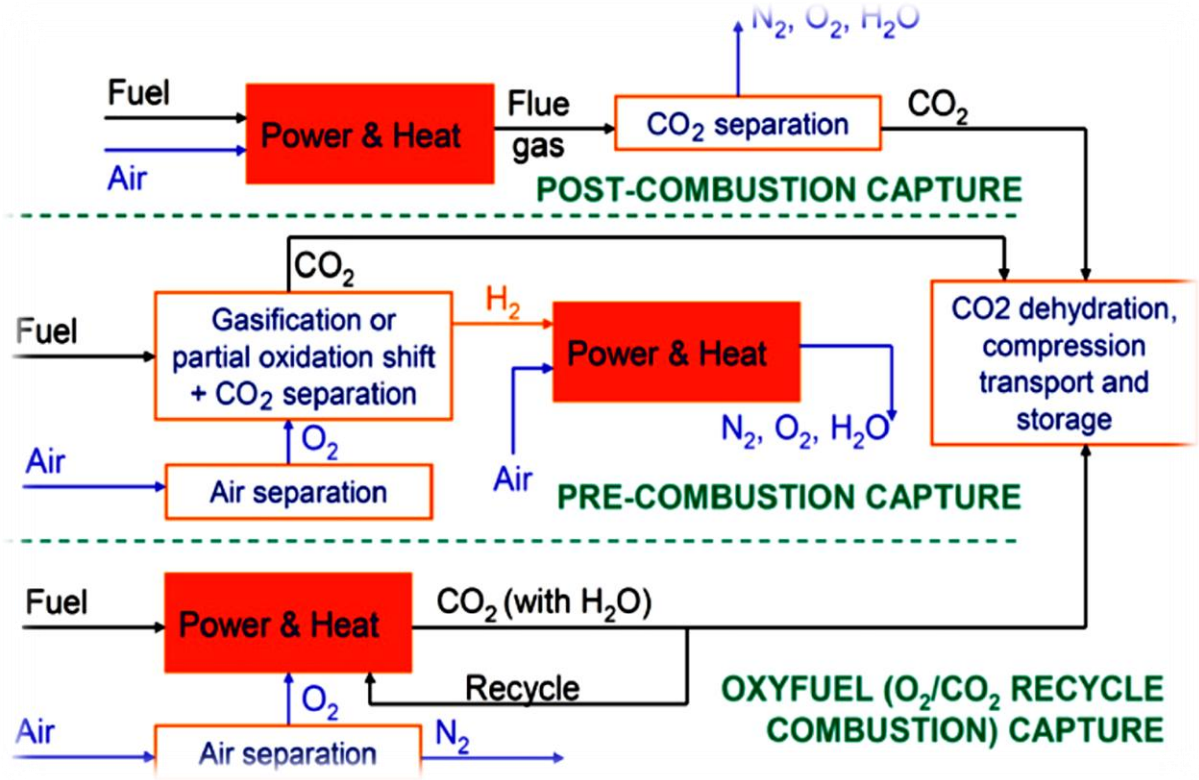

Figure 1.1 Operating Principles of CO_2 capture technologies (Gibbins & Chalmers., 2008)

1.2.1.1 Pre-combustion CO_2 capture

Pre-combustion technique employs the extraction of carbon before its burning. Fuel is gasified using oxygen which produces synthetic gas (a mixture of CO and H_2). Carbon monoxide is converted into CO_2 along with additional production of H_2 by using steam. CO_2 can be chemically separated out.

1.2.1.2 Post combustion CO_2 capture

This technology is particularly suited to retrofit applications. For post-combustion capture, CO_2 is removed after the combustion of the fuel. CO_2 is contained in the flue gas from combustion. Usually a chemical solvent is used to capture the CO_2 from the flue gas. This solvent is regenerated by heating and CO_2 is compressed, transported and stored. Energy is required for stripping of CO_2 from the solvent.

1.2.1.3 Oxy-fuel combustion

This technology employs the oxygen as gasification media instead of air. The oxygen obtained from air by separation techniques. The result of this gasification will be a very low amount of CO_2 in the flue gases and CO_2 can be easily separated.

1.3 Gas separation methods for CO_2 capture:

CO_2 can be separated from flue or stack gas by employing different methods as follows:

- Chemical and Physical absorption
- Physical adsorption
- Membrane technologies
- Cryogenic separation

The selection criteria for these methods depend upon capture effectiveness, process economy, and energy consumption.

1.3.1 Chemical absorption

This method utilizes the different reactivity's of various gases with sorbents to separate them. MEA and other amines are used as sorbents for this method. The reactions should be reversible so that sorbent can be regenerated. This method was originally used for CO_2 removal from methane, hydrogen etc.

1.3.2 Physical absorption

In this method, CO_2 molecules dissolved in solvent and bonded with solvent molecules without any chemical reaction. The amount of gas absorbed increases linearly with increase in its partial pressure. Physical absorption is more effective if partial pressure of the absorbed gas is high. It also depends upon the temperature. Lower is the temperature, more gas is absorbed.

1.3.3 Physical adsorption

Gas is adsorbed on the solid surface by Van der Waal forces. Separation is based on the difference in gas molecule sizes or different binding forces. Pressure and temperature swing adsorption methods are used. The most common adsorbents are activated carbon, silica gel and aluminum oxide (Folger., 2010).

1.3.4 Membrane technologies

The principle behind this method is the applied pressure. Some of the gas molecules will pass through the micro pores of membranes and some will not. The driving forces for this separation are hydrostatic pressure and concentration gradients.

1.3.5 Cryogenic separation

Difference in the boiling points of various gases is the basic principle behind this method. All the gases have different boiling points and this method provide effective gas separation.

1.4 CO_2 transport and storage

Carbon sequestration (storage) is the isolation of carbon dioxide (CO_2) from the earth's atmosphere. One method is to store CO_2 underground in rock formations. CO_2 can be stored there for long period of time. The CO_2 would remain in small pore spaces inherent in rocks. These pore spaces contain traces of oil and natural gas. It would enhance oil recovery from reservoirs. CO_2 will be transported through pipeline or ships.

1.5 Research and future for CO_2 capture

All the three CO_2 capture technologies are capable of high efficiencies (about 90%). But the major drawback for these technologies is high cost and energy requirements. At present, there is no existing plant running with CO_2 capture technology. To overcome this problem, a number of both gas and coal fired gasification power plants are underway in US and Europe. Research and development is necessary to find the best method and solvent in the form of low cost and low energy requirements for CO_2 capture. R&D focus is on developing new novel solvents, sorbents, membranes

and oxy fuel systems. Technology roadmaps have been developed in the world for the availability of commercial deployment of CO_2 capture by 2020 (**Fogler, 2010**).

1.6 Motivation and Scope of Work

The processes used for the removal of CO_2 from natural gas and industrial gas streams are the regenerative absorption of CO_2 into aqueous solutions of alkanolamines. Commercially important alkanolamines used for this purpose are mono-ethanolamine (MEA), di-ethanolamine (DEA), N-methyl di-ethanolamine (MDEA), and 2-amino-2-methyl-1-propanol (AMP) (Kohl & Nielsen., 1997)**.** The gas streams in these processes are usually at high pressures of about 3 to 10 MPa. However, the major challenges for CO_2 capture from fossil fuel based power plants are the large volumetric flow rates of flue gas at essentially atmospheric pressure with large amount of CO_2 at low partial pressures. The presence of SO_x, NO_x, and significant oxygen partial pressure in the flue gas from coal based power plants gives rise to further problems for implementation of the amine absorption process for CO_2 capture from power plant flue gas streams. The MEA is considered suitable for flue gas cleaning because of its high reaction rate at low CO_2 partial pressure and low raw material cost. But the disadvantages of using MEA are high absorption because of the high energy consumption in regenerating and operation problems such as corrosion, solvent loss, and solvent degradation (Gabrielsen et al., 2006). Furthermore, MEA can be loaded up to only 0.5 mol of CO_2 per mol MEA as a result of the stable carbamates formed (Gabrielsen et al., 2007)

Then a new class of amines, sterically hindered amines was reported by Sartori (Sartori et al., 1983), that can be commercially attractive as new absorbent for CO_2 capture process. It was observed that the steric effect influence the stability of the carbamates due to the amine-CO_2 reaction and proposed the use of highly branched amines such as AMP for higher cyclic absorption capacity for CO_2 (Sharma., 1964). As in MDEA, the CO_2 loading in AMP approaches a value of 1.0 mol of CO_2 per mole of amine, while the reaction rate constant for (CO_2 + AMP) is much higher than that for (CO_2 + MDEA). Since the sterically hindered amine does not form a stable carbamate, bicarbonate and carbonate ions may be present in the solution in larger amounts than carbamate ions (Saha et al,. 1995). Hence, the cost of regeneration energy for AMP is less than MDEA. The regeneration performance can be ranked in the following order: AMP > MDEA > DEA > MEA. That is why AMP is the most important sterically hindered amine for CO_2 removal from natural gas as well as from power plant flue gas (Gabrielsen et al., 2007).

The VLE data of the (CO_2 + amine + water) system at various temperatures and concentrations have a very important role in the design and optimization of industrial gas treating processes. In this situation, VLE experiments data can be used by the designer and a basis for with elaborate care can

produce a data bank which can not only serve the designer but also can provide a base for thermodynamic prediction models. Obtaining such data can only be successful with a reliable and validated experimental set up, standard procedures and accurate computational methods.

This study report is the extension of the autumn research work. The autumn project work presented low pressure/temperature VLE experiments for 3M AMP and 1.5M PZ. This study report presents low and high pressure VLE of the AMP-CO_2-Water and high pressure VLE of PZ-CO_2-Water systems. The partial pressure of carbon dioxide has been measured over aqueous AMP (0.1M, 1M and 3M) and aqueous PZ (1.5M) solutions at different temperature ranges, are listed in table 1.1. A rigorous thermodynamic VLE model (e-NRTL) is also developed for AMP-CO_2-H_2O system to start learning with the simple case. A thermodynamic property model capable of accurate representation of the vapor liquid equilibrium (VLE) of the aqueous AMP−CO_2 system is essential for a successful computer simulation of the process. Accurate speciation of the solution is an integral part of the equilibrium calculations, therefore, a robust thermodynamic model at all possible combinations of temperature, amine concentration, and acid gas loading is needed.

The objective of modeling part of this work is to experimentally determine the VLE of CO_2 in aqueous AMP and validate the e-NRTL model developed by (Chen and Evans., 1986) with the help of in-house experimental results and available literature over a wide range of amine concentration, CO_2 loading, CO_2 partial pressure and temperature.

Table1.1 VLE data obtained for AMP during this work

System	Temperatures (^{0}C)	Loading (mol CO_2/mol amine)	CO_2-partial pressure (kPa)	Total pressure (kPa)
3M AMP-CO_2-H_2O	40, 60 & 80^{0}C 80, 100 & 120^{0}C	0.01-0.72 0.17048-0.9318	0.0162-17.4055	222.4-973.9
1.5M Pz-CO2-H_2O	40,60 & 80^{0}C 100 & 120^{0}C	0.05-0.53 0.1723-0.8987	0.03-15.5350	222.4-973.9
0.1M AMP/CO2/H_2O	40,60& 80 100 & 120	0.0998-1.0395 0.7615-1.9485	0.0270-9.0375	245.20-994.90
1M-AMP-CO_2- H_2O	40,60& 80 100 & 120	0.067-0.8533 0.2373-0.9786	0.0427-18.6703	269.8-1001.9

1.7 Basic chemistry and kinetics of amine

Generally, alkanolamines amines have one hydroxyl group and one amino group. In general it can be considered that the hydroxyl group serves to reduce the vapor pressure and increases solubility in water, while the amino group provides the necessary alkalinity in water solutions to cause the absorption of acidic gases. Each alkanolamine has at least one hydroxyl group and one amino group (Kohl & Nielsen, 1997).

The main types of the amines are as follows:

1.7.1 Primary amine

Amines in which one hydrogen atom from the ammonia molecule is replaced with organic compound or Amines which have two hydrogen atoms directly attached to a nitrogen atom, such as monoethanolamine (MEA) and 2-(2-aminoethoxy) ethanol (DGA). These are generally the most alkaline.

Figure 1.2 Primary amines MEA (left) and DGA (right) (Kohl & Nielsen, 1997)

1.7.2 Secondary Amine

Amines in which two hydrogen atoms from the ammonia molecule is replaced with organic compounds Amines in which there is only one hydrogen attached to nitrogen for example di-ethanolamine (DEA) and di-isopropanol-amine (DIPA).

Figure 1.3 Secondary amines DEA (left) and DIPA (right) (Kohl & Nielsen, 1997)

1.7.3 Tertiary Amine

The amines in which three hydrogen atoms from ammonia molecule are replaced with organic compounds or Tertiary amines represent completely substituted ammonia molecules with no

hydrogen atoms attached to the nitrogen for example tri-ethanol-amine (TEA) and methyl-di-ethanol-amine (MDEA).

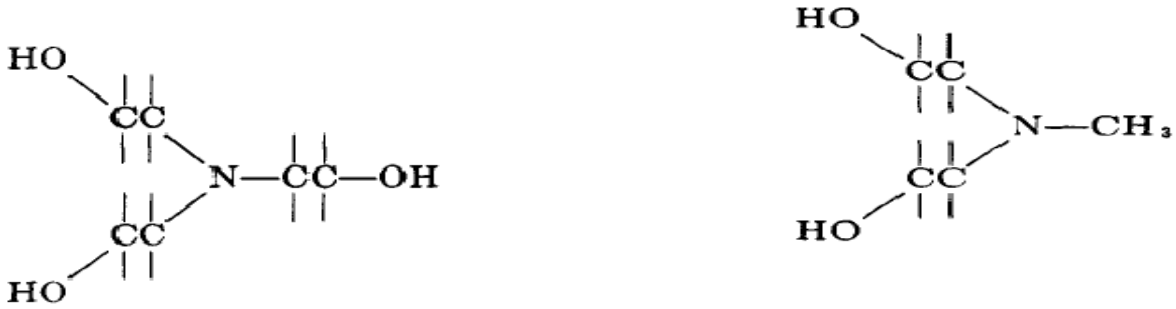

Figure 1.4 Tertiary amines TEA (left) and MDEA (right) (Kohl & Nielsen, 1997)

1.7.4 Sterically hindered amines

A sterically hindered amine is defined as a primary amine in which an amino group (NH2) is fixed to a tertiary carbon atom, or a secondary amine in which the amino group is fixed to a secondary or tertiary carbon atom. This type of amine does not form stable form of carbamate (Mandal and Bandyopadhyay 2006).

Figure 1.5 Sterically hindered amines 2-amino-2-methyl-1-propanol (AMP) (left) and 2- Piperidine ethanol (PE) (right) (Kohl & Nielsen, 1997)

Chapter 2

Materials and Experimental Techniques

2.1 Materials

2.1.1 Solutions and calibration gases

Sigma Aldrich sold AMP (≥ 97%) with CAS no 124-68-5 and Piperazine (≥ 98%) with CAS no 110-85-0 under different brand names, the one used in these experiments has purity of greater than 97 % (fluka). AMP with concentration (0.1, 1 and 3)M was prepared by using de-ionized water with great care. There might be impurities that can react with CO_2 but still since the purity is high so impurities have no significant effect.

The CO_2 (purity > 99.999 mol % from AGA Gas GmbH) and Nitrogen N_2 (purity > 99.999 mol% from YARA PRAXAIR) were used for calibration, flushing and loading. Calibration gas (4.96 mol% CO_2 from AGA Gas GmbH and 100ppm from YARA PRAXAIR) was used to calibrate the IR CO_2 analyzer (1 and 2) of atmospheric pressure equipment after using them each time or on daily basis and flushing them with N_2 after finishing experiments for the day.

2.1.2 Chemicals for CO_2 and Amine Analyses

Standard Solutions

0.1N NaOH (ampoule for 1000 mL supplied Merck KGaA)

0.1N HCl (ampoule for 1000 mL supplied Merck KgaA)

0.2N H_2SO_4 (2, 0.1 ampoules for 1000 mL supplied by Merck KgaA)

1N $BaCl_2$ (244 g $BaCl_2.2H_2O$/2L with purity > 99% supplied by SIGMA-ALDRICH) All standard solutions were prepared from above mentioned chemicals and de-ionized water.

Filters 0.45µmHAWP supplied by MILLIPORE

2.2 Experimental setup

2.2.1 Low pressure (Atmospheric) VLE apparatus

VLE (Vapor–liquid equilibrium) for the CO_2 loaded amine systems from 40 to 80 °C at atmospheric pressure were measured using a low temperature/atmospheric vapor–liquid equilibrium apparatus (see Fig. 2.1), designed to operate up to 80±0.1 °C. It consists of four 360-cm^3 glass flasks. The apparatus placed in a thermostat box is equipped with heater, fan, water bath, mixing feed controller, IR analyzers, condenser and gas phase pump. During the experiment, 150 cm^3 of pre-loaded sample solution was fed into flask 2, 3 and 4, while flask 1 was used as a gas stabilizer/ liquid lock. The flasks were heated in the water-bath and placed in a thermostat box with the controlled temperature within ±0.1°C.

K-type thermocouples were used to record the temperature in the cell, the water-bath and the gas phase temperature between the condenser and the analyzer respectively. The gas phase was circulated by a BUHLER pump (model2) to reach the desired level. The procedure was improved from the previous works (Ma'mun, et al., 2005), i.e. during the circulation of gas phase, the line to the analyzer was closed during equilibrium to minimize the condensates after cooling water, when the equilibrium is almost reached (usually up to 20-25 minutes), then the line to the analyzer was opened. The vapour bleed extracted for composition measurement was cooled to 12-15 °C to condense water and amine, and the CO_2 content was directly determined by IR analyzer.

The IR analyzers were calibrated every time before or after use. Four IR CO_2 analyzers (0-20 %; 0-5 %; 0-1 % and 0-2000ppm) were used to measure gas phase CO_2 content accurately. Two different purity of CO_2 (i.e. 99.999% and 4.985%) were blended with N_2 to obtain a desired level of CO_2 in the analyzer. Liquid phase composition of CO_2 was obtained by taking a 25cm^3 sample from cell 4 for CO_2 analysis by the barium chloride method and amine analysis for total alkalinity. The liquid phase in all the cells were removed and diluted with fresh solution or loaded with more CO_2 to change to a new loading. Than the equilibrium cells were refilled with new solutions for further measurements.

The vapour phase in the IR analyzer, will consist of N_2, CO_2, and small amounts of H_2O and AMP. The measured concentration of CO_2 in the IR-analyzer is then

$$y^{IR}co_2 = \frac{\mathrm{n}^{\mathrm{IR}}{}_{\mathrm{co2}}}{\mathrm{n}^{\mathrm{IR}}_{\mathrm{CO2}} + \mathrm{n}^{\mathrm{IR}}_{\mathrm{N2}} + \mathrm{n}^{\mathrm{IR}}_{\mathrm{H2O}} + \mathrm{n}^{\mathrm{IR}}_{\mathrm{amine}}} \qquad (2.1)$$

where n is the molar flow and the superscript IR is the vapor phase in the IR analyzer.

The circulating vapour phase in the system consisted of N_2, CO_2, and significant amounts of H_2O and AMP. As CO_2 and N_2 are non condensable gases, so the flow of CO_2 and N_2 were the same before and after the condenser. The amount of condensate observed at 40 and 60 ^{0}C was too small to perform CO_2 and amine analysis but at 80 ^{0}C considerable amount (10 gm) was collected. The CO_2 and amine concentrations were checked and found to have a negligible influence on the results even at low CO_2 partial pressure. Equation 1 together with a mole balance will give the molar flow of CO_2 in the system

$$y^{IR}co_2 = \frac{n_{co2}}{n_{total} - \left(n_{H2O} + n^{IR}_{H2O}\right) - \left(n_{Amine} - n^{IR}_{amine}\right)} \qquad (2.2)$$

Where n_{tot} n_{H2O}, and n_{Amine} respectively, denote the total molar flow and the molar flows of H_2O and Amine in the circulation system.

$$P_{CO2} = y^{IR}_{CO2}\left[P - \left(P_{H2O} - P^{IR}_{H2O}\right) - \left(P_{amine} - P^{IR}_{Amine}\right)\right] \qquad (2.3)$$

The partial pressure P_{H2O}, P^{IR}_{H2O}, P_{Amine} and P^{IR}_{Amine} could be determined using the model and where available total vapor pressure of the amine is used according to the eq. 2.4

$$P_{CO2} = y^{IR}{}_{CO2}\left[P - \left(P_{T\,solution} - P^{IR}{}_{T\,solution}\right]\right. \qquad (2.4)$$

where $y^{IR}{}_{CO2}$ is the mole fraction of CO_2 in the analyzer ; P is the total pressure in the equilibrium cell; $P_{Tsolution}$ is the vapor pressure of solution at the cell temperature and $P^{IR}_{solution}$ is the vapor pressure of the solution at cooler temperature and these pressure can be determine by ebulliometer measurements.

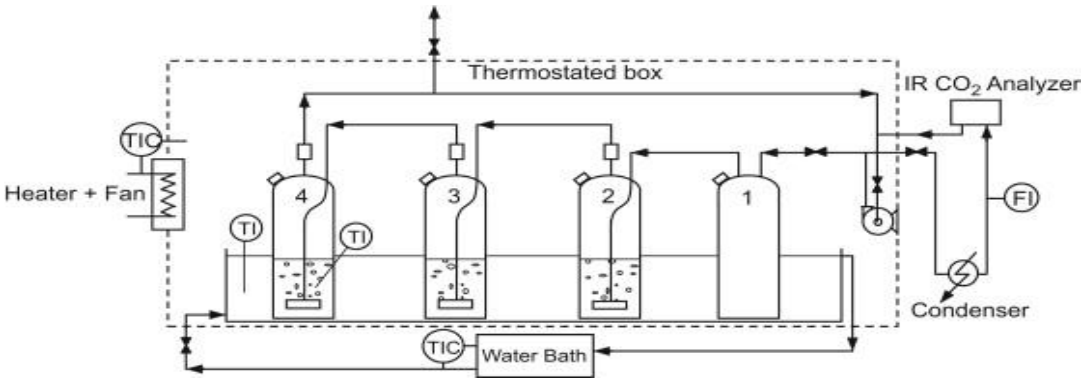

Figure 2.1 Low temperature/atmospheric vapor–liquid equilibrium apparatus (Ma'mun, et al., 2006)

2.2.2 High pressure VLE apparatus

High pressure/temperature VLE (vapour liquid equilibrium) apparatus was used to measure the vapour liquid equilibrium for the system (0.1M, 1M and 3M) AMP as shown in Figure 2.2. The

apparatus consists of two connected autoclaves (1000 and 200 cm^3) which rotate at 180° to and forth with 2 rpm and are designed to operate up to 2 MPa and 150 °C. A Druck PTX 7517-1 (10 bar abs) pressure transducer, and two K-type thermocouples were used to measure the pressure and temperature. This apparatus was used for high pressure amine vapour-liquid equilibrium measurements, as for high pressure low VLE apparatus cannot be used because of its pressure and temperature limitations.

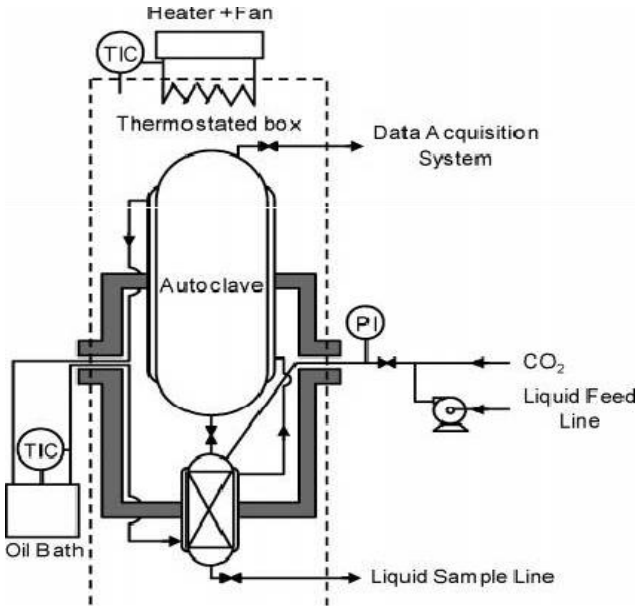

Figure 2.2 Vapor-liquid equilibrium apparatus 1for High Pressure (Ma, 'mun et al., 2005)

Before starting the experiment (first time) the apparatus was rinsed with a hot water and de-ionized water. To remove any water in the reactor, a fresh prepared solution was used, e.g. (0.1M, 1M,3M AMP) several time to rinse the apparatus. Any water in the reactor could reduce the concentration of amine. Before starting the experiment, the oil bath and the heating of cabinet (a thermostat box) were switched on. During the heating-up period, the autoclaves were purged with CO_2 several times.

The unloaded amine solution of 200ml was then injected into the smaller autoclave. When the temperature reached below 10 ^{0}C (almost), CO_2 was injected to the desired pressure for two hrs. Equilibrium was obtained when the temperature and pressure were constant to within ±0.2 °C and ±1 kPa. This took approximately 5 to 6 hrs. After equilibrium was obtained, i.e. when temperature and pressure were constant, a liquid sample for analysis was collected by closed sampling into a sampling cylinder containing about 100 mL of fresh solution. This immediately reduces the CO_2 pressure and CO_2 loss is avoided. The cylinder was weighed before and after sampling and put into the refrigerator at below ambient temperature. It was done to ensure no loss of CO_2 by flashing at atmospheric pressure. The actual CO_2 loading is determined by titration analysis and mass

balance. This apparatus was used to measure the total pressure, the partial pressure of CO_2 was estimated by subtracting the partial pressures of solution (H_2O and Amine) from the total pressure.

2.2.3 Ebulliometric measurements

The vapor pressure and temperature data for aqueous AMP with different concentrations was obtained by experimentation on modified Świętosławski ebulliometer. The experimental scheme and apparatus are shown in the figure 2.3 b. The equilibrium still has a volume of 200 mL and is designed for operation at max temperature and pressure of 200^0C and 1 bar respectively. Pt-100 resistance thermo-sensor with an uncertainty of (±0.05 K) was used to measure the temperature in the equilibrium still while the pressure was measured with a calibrated DPI520 pressure controller with an uncertainty of ±0.3 kPa.

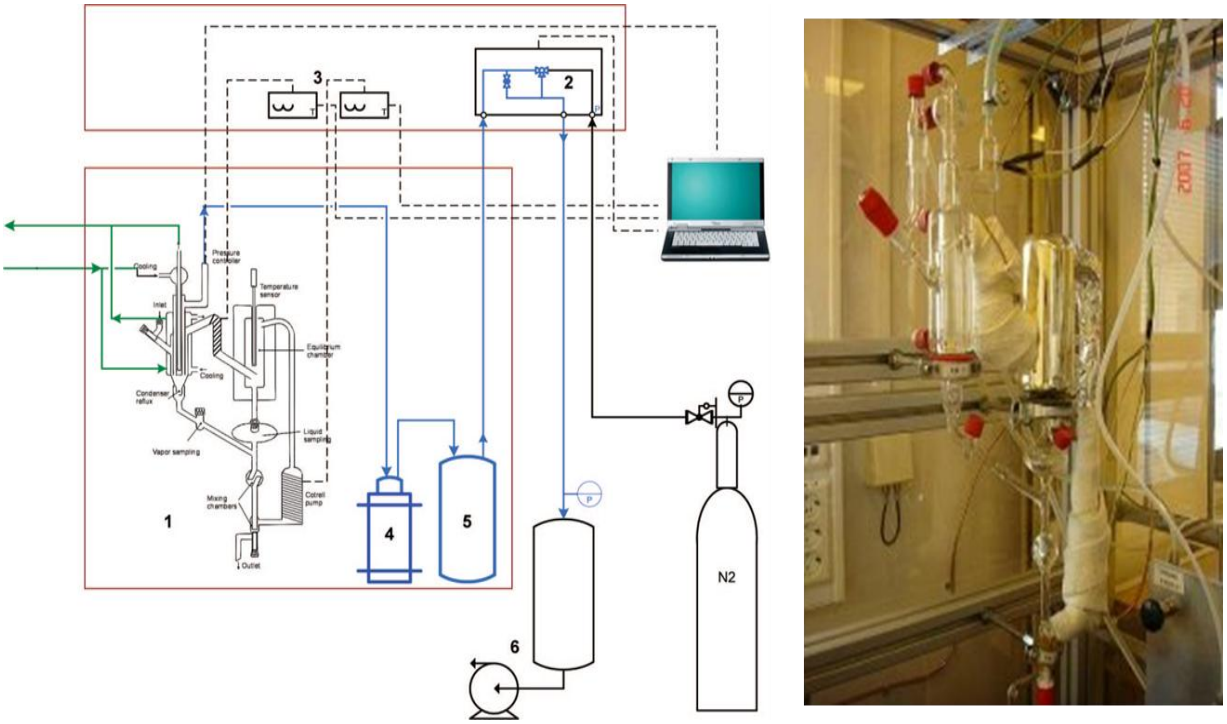

Figure 2.3 Experimental setup: 1, ebulliometer ; 2, pressure controller; 3, temperature controllers; 4, cold trap; 5, buffer vessel; 6, vacuum pump with a buffer vessel (Kim et al., 2009)

Ebulliometer can be run under either isothermal mode or isobaric mode. In isobaric mode pressure is kept constant and temperature is changed while in case of isothermal mode, temperature is kept constant and pressure is changed to get the equilibrium. Isothermal mode was adapted for present measurements. First, ebulliometer was charged with 85-90ml of the desired amine solvent/solution to measure the boiling temperatures and vapor pressure and then purged it with nitrogen.

Pressure was lowered and checked the apparatus for any leakages by seeing the fluctuation in pressure operating line for very low pressure inside ebulliometer. Pressure was adjusted gradually to get the desired temperature. The liquid will be heated and evaporated partially. The Cottrell pump carries the overhead liquid and vapor condensate to equilibrium chamber.

This process continued until equilibrium was established with smooth boiling and temperature was almost a constant value (with fluctuations not more than ±0.05K) for more than ten minutes after this. This was the required value of equilibrium temperature. Liquid and vapor condensate samples (5 and 1ml respectively) were collected using disposable plastic syringes from liquid and vapor phase sampling ports. Sampling ports were sealed with silicon septa. The make-up of the solution was done. In this way, experiment was repeated to get the vapor pressure data at different temperatures. Antoine equation was used to measure saturation pressure as shown below:

$$\log_{10} P = A - \frac{B}{T+C} \qquad (2.5)$$

2.2.4 Solubility Measurements

Determination of the free CO_2 solubility in aqueous amine solutions at various concentrations and temperatures is essential for developing a kinetic model and also for correct implementation of the system thermodynamics. Due to the reactive nature of any absorbent with CO_2, it is not possible to measure the solubility of CO_2 in the absorbent solutions directly. This property can, however, be estimated indirectly from corresponding data of similar non-reacting gases using N_2O analogy. The solubility of CO_2 can be inferred using the N_2O analogy, originally proposed by (Clark, 1964), verified by (Laddha et al., 1981) and frequently used for various amine systems.

2.2.4.1 Experimental procedure

The physical solubility of N_2O into loaded amine (3M AMP with different loading 0.1, 0.3 and maximum) system was performed with the apparatus shown in Fig 2.4. The apparatus consists of a stirred jacketed glass vessel of volume ($1*10^{-3}m^3$) and a stainless steel gas holding vessel of calibrated volume ($1.17*10^{-3}$ m^3). A known mass of solvent was weighed and transferred to the glass vessel (about half of the reactor volume). The solution was thereafter degassed by vacuum around 2 kPa at ambient temperature until vapor-liquid equilibrium was established. To minimize the solvent losses during degassing, the glass vessel was equipped with an outlet condenser and a cooling medium at around 4.0 ^{0}C was circulated using a Julabo F25 water bath. During the solubility measurements, cooling system was switched off and the gas outlet closed. The reactor was heated to the desire temperature by a heating medium circulating through a Lauda E300 oil bath with a

temperature uncertainty ±0.1 °C. After degassing the initial temperature and pressure in the reactor and in the N_2O gas holding vessel were recorded.

Figure 2.4 Experimental setup for solubility measurements

The commercial N_2O gas was supplied by AGA Gas GmbH with a purity of 99.999% and was added to the reactor by shortly opening the valve to the steel gas holding vessel. Equilibrium was then established afterabout 4-5 hours and the pressure recorded by two pressure transducers (Druck PTX 610 and PCE-28 with uncertainty ± 0.08 % (800 kPa) and ± 0.1% (600 k) of full scale, respectively). Two K type thermocouples recorded the temperatures in the jacketed glass vessel and in the stainless steel gas supply vessel respectively, with uncertainty ±0.1 ºC. All data were acquired using a FieldPoint and LabView data acquisition system.

At equilibrium, the partial pressure of N_2O (P_{N2O}) is taken as the difference between the total pressure in the reactor (PR) and the solvent vapor pressure (Ps). Where the solvent pressure is the total pressure measured in the reactor before adding N_2O. The assumption made is that the added N_2O does not change the vapor pressure of original solution.

$$P_{N2O} = P_R - P_s^o \quad (2.6)$$

The total amount of N_2O added was calculated from the difference between the initial and final pressure of the gas supply vessel before and after feeding N_2O as:

$$n_{N2O}^{added} = \frac{V_v}{RT_v}\left[\frac{P_{v1}}{z_1} - \frac{P_{v2}}{z_2}\right] \quad (2.7)$$

Where P_v is pressure, T_v is temperature, V_v is volume of the stainless steel N_2O gas holding vessel, z is the compressibility factor of the gas and R is the gas constant. Subscript 1 and 2 are the initial and final conditions respectively. The amount of N_2O in the gas-phase at equilibrium, n_{N2O}^{g} was calculated as:

$$n_{N2O}^{g} = \frac{P_{N2O}}{z_{N2O}RT_R}(V_R - V_s) \quad (2.8)$$

Where V_r, V_s and z_{N2O} are the total reactor volume, volume of the solvent and compressibility factor for N_2O respectively. The density of the solvent is needed to calculate the solvent volume Vs and compressibility factor is calculated by using the Peng-Robinson equation of state. The density data was measured by Muhammad Usman (master student at NTNU in CO_2 capture group).

The absorbed amount of N_2O into the liquid phase can then be calculated as the difference between N_2O added, n_{N2O}^{added} and the increase of N_2O in the gas-phase, n_{N2O}^{g}. Thus the concentration of N_20 in the liquid phase C_{N2O}^{l} is calculated as:

$$C_{N2O}^{l} = \frac{n_{N2O}^{added} - n_{N2O}^{g}}{V_s} \quad (2.9)$$

The solubility was expressed by a Henry's law constant according to the equation:

$$P_{N2O} = H_{N2O} \cdot C_{N2O}^{l} \quad (2.10)$$

A titration analysis for measuring the total CO_2 content in the sample before and after the measurement was performed. The difference in loading before and after the measurement was found to be 6 % maximum.

2.3 Analysis of liquid samples

All liquid samples were analyzed for CO_2 and amine concentrations by precipitation titration method. The apparatuses used for amine and CO_2 concentrations are shown in the figure 2.5 (a) and 2.5 (b) respectively.

2.3.1 CO_2 analyses of liquid samples

Liquid samples containing CO_2 were analyzed by the precipitation titration method. The liquid sample was added to a 250 cm^3 Erlenmeyer flask containing 50 cm^3 sodium hydroxide (0.1 N NaOH) and 25 cm^3 barium chloride (1 N $BaCl_2$) solution. The amount of the liquid sample added dependent on the total CO_2 content in the sample. The Erlenmeyer flask was heated to enhance the barium carbonate ($BaCO_3$) formation and then cooled to ambient temperature. The mixture was filtered with a 0.45 µm Millipore paper and washed with de-ionized water. The filter covered by $BaCO_3$ was transferred to a 250 cm^3 beaker. De-ionized water (100 cm^3) was added into the beaker, and enough hydrochloric acid (0.1N HCl) was added to dissolve the $BaCO_3$ cake. The amount of HCl which was not used to dissolve $BaCO_3$ was then titrated with 0.1 N NaOH in an automatic titrator (Metrohm 809 Titrando).The Metrohm 809 Titrando is shown in the figure 2.5(a) with an end-point of pH 5.2. After the titration, the following equation was used to calculate the amount of CO_2 in the liquid phase.

$$CO_2(mole/kg) = \frac{1}{20} \cdot \frac{HCl(gm) - NaOH(ml) - [\text{Blank}HCl(gm) - \text{Blank}NaOH(ml)]}{\text{Sample}(gm)}$$

$$CO_2(mole/liter) = CO_2(mole/kg) \cdot \rho_{sol}(kg/liter)$$

Figure 2.5(a) The Metrohm 809 Titrando for CO_2 analysis

After ferforming two parallel sample of CO_2 analysis, the uncertainty in measuring the CO_2 concentration was found less than 2%.

2.3.2 Amine analysis of liquid samples

50ml of liquid sample was collected in sampling bottles during the experiments. Titration apparatus used was Mettler Toledo G-20 as shown in the figure 2.5(b). High concentration samples were analyzed by using 0.2N H_2SO_4 as titrant and low concentration samples were analyzed by using $0.02NH_2SO_4$. There was no hard and fast rule for low concentrations of the samples. If the titrant used is very low and less 2ml then remaining low concentration samples were analyzed using other titrant of low concentration. The advantage of this apparatus is that one can save time by placing 9 samples at one time and it works automatically.

Preparation of sample for analysis

60 ml of distilled water was added to sampling beaker, tare it and 0.2- 0.4ml of sample was added depending upon the estimated sample concentration. The weight of the sample was noted. Two Parallel samples were prepared for each point. Uncertainty in measuring the amine analysis was found less than 2%.

How to run the program

LabX software program was used for determination of the amine concentrations by titration. Weighed quantities of the sample are filled there and program was started. Results were obtained for amine concentration in mol/Kg.

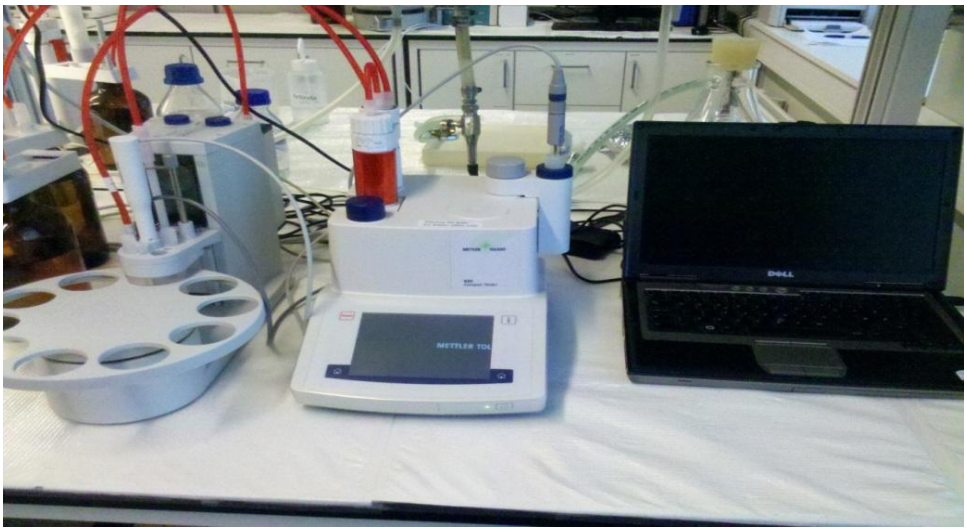

Figure 2.5(b) Mettler Toledo G-20 setup for amine analysis

2.4 Calibration of the equipments

2.4.1 High pressureequipment

For high-pressure equipment, since the thermocouple and pressure transducer weres calibrated once so it's not necessary to calibrate every time and those calibration data was already fed into computer which was selected before starting the software Labview.

2.4.2 Calibration of CO_2 analyzer

All analyzers were calibrated every time after using each analyzer. The actual concentrations of CO_2 were obtained from the calibration curve drawn for actual CO_2 Vol % vs Volts of IR analyzer as shown in figure 2.6.

Figure 2.6 shows an example for analyzer calibration and the equation of the line which is basically used to calculate error free Vol% CO_2.

All the observations and CO_2 analyses along with amine analyses were put in an excel sheet to calculate the CO_2 loading as mol of CO_2/mol of amine which will be discussed in results and discussion. The partial pressure of CO_2 was calculated by subtracting partial pressures of water and amine at given temperature from the atmospheric pressure obtained from barometer.

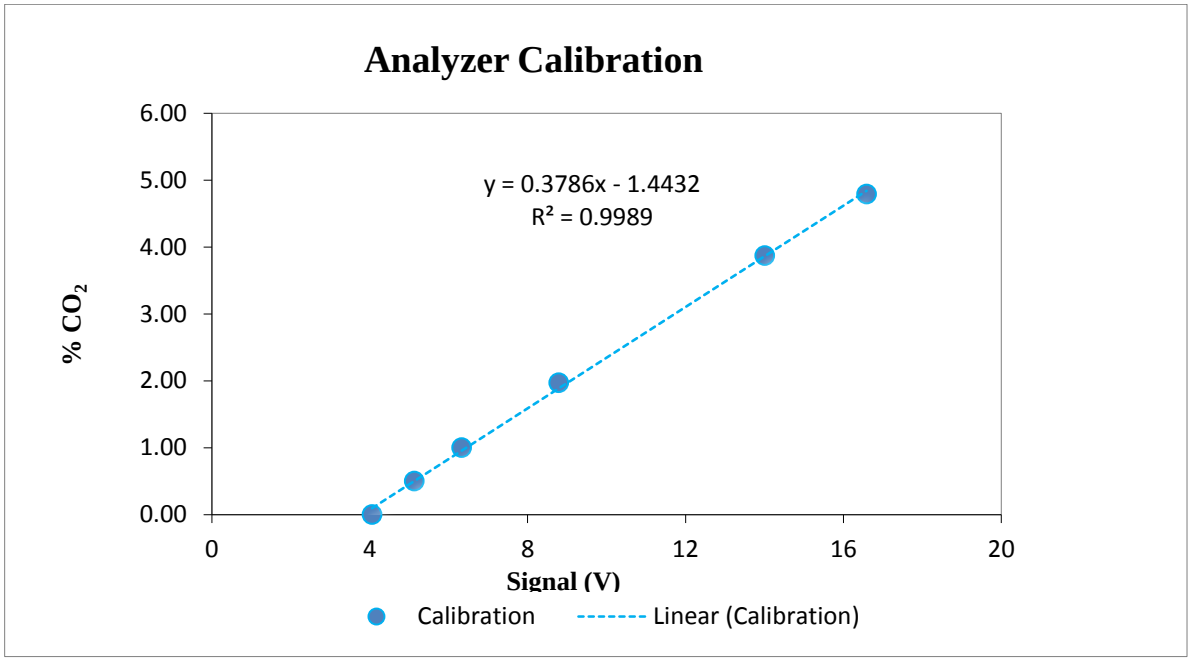

Figure 2.6 Analyzer Calibration (e.g. for Channel 3)

Chapter 3

Thermodynamic Framework

3.1 Introduction

Thermodynamic concepts that have been applied in this work are discussed in this chapter. Explanation of phase and chemical equilibria, activity and activity coefficients, fugacity and fugacity coefficients and relations between them are presented. Most of the discussions that follow in this section can be found in various thermodynamics textbooks (e.g. Denbigh, 1984; Prausnitz et al., 1999; Elliot et al., 1999). The process for the absorption of gas component goes into two steps. In first step the gas phase species dissolve in the aqueous phase:

$$CO_{2(g)} \longleftrightarrow CO_{2(l)} \qquad (3.1)$$

In the second step the chemical reaction serves to convert the aqueous phase species into ions and pull the reaction 3.1 in the forward direction. For more explanation see figure 3.1.

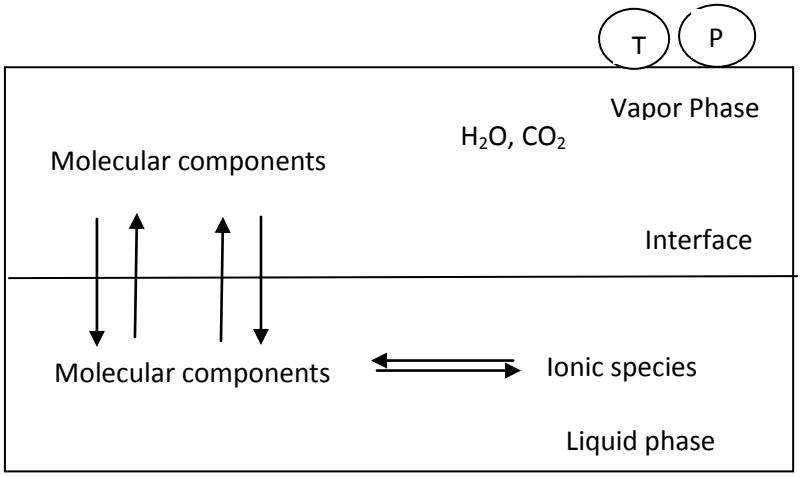

Figure 3.1 Chemical and phase equilibria

VLE model is based on phase equilibrium conditions for neutral species and chemical equilibria for all elementary chemical reactions in the system. Both CO_2 in the liquid phase and alkanolamines are weak electrolytes. As such they partially dissociate in the aqueous phase to form a complex mixture of nonvolatile or moderately volatile solvent species, highly volatile acid gas (molecular species), and non-volatile ionic species. The equilibrium distribution of these species between a vapor and liquid phase is governed by the equality of their chemical potential among the contacting phases. Chemical potential or partial molar Gibbs free energy is related to the activity coefficient of

the species through partial molar excess Gibbs free energy. An activity coefficient model (or excess Gibbs energy model) is an essential component of VLE models.

3.2 Thermodynamic Equilibrium

For a close vapor-liquid system the fundamental criterion for phase equilibrium may be summarized as follows:

$$T^V = T^L \qquad (3.2a)$$

$$P^V = P^L \qquad (3.2b)$$

$$\mu_i^V = \mu_i^L \qquad (3.2c)$$

It states that at equilibrium, the temperature, pressure and chemical potential of all species in vapor and liquid phase are uniform over the whole system. The task of phase equilibrium thermodynamics is to describe quantitatively the distribution at equilibrium of every component among all the present phases. The chemical potential does not have an immediate equivalent in the physical world it is therefore desirable to express the chemical potential in terms of some auxiliary function that might be more easily identified with physical reality (Prausnitz et al., 1999). The term fugacity (f) was introduced by G.N. Lewis to transform the chemical potential to a fugacity term discus below.

3.2.1 Fugacity and Fugacity Coefficient

The fugacity of component i in a mixture at constant T for any system, Solid, Liquid, gas, pure mixed ideal or non ideal is,

$$\mu_i - \mu_i^o = RT\ ln\frac{f}{f_i^0} \qquad (3.3)$$

Where μ_i^o and f_i^0 are for the pure fluid at the system temperature and may not be chosen independently. When one is chosen the other is fixed. Writing an analogous expression for the liquid phase and equating the chemical potential of liquid and vapor phases using equation (3.2c) we find:

$$\mu_i^V - \mu_i^L = RT\ ln\frac{f_i^V}{f_i^L} = 0 \qquad (3.4)$$

When the reference state of both the fluids is the same then, $\mu_i^{0V} = \mu_i^{0L}$, this leads to additional criteria that can be written as:

$$f_i^L = f_i^V \qquad (3.5)$$

Equation (3.5) tells us that the equilibrium conditions in terms of chemical potential can be replaced wit out loss of generality by an equation in terms of fugacity.

Fugacity has a unit of pressure and has a direct relation to the chemical potential. For a pure ideal gas fugacity is equal to the pressure and for a component i in mixture of ideal gas, it is equal to the partial pressure y_iP. At very low pressure for all system, the gas behaves like an ideal gas and fugacity is equal to the partial pressure. The definition is completed by the limit.

$$\frac{f_i}{y_i P} \to 1 \; as \; P \to 0 \qquad (3.6)$$

The fugacity coefficient is the ratio of fugacity to real gas pressure. It is a measure of non ideality. It is simply another way of characterizing the Gibbs excess function at fixed T,P. For a mixture of ideal gases $\emptyset_i$ =1

$$\frac{f_i}{y_i P} = \emptyset \mathrm{i} \qquad (3.7)$$

There are two ways to calculate the fugacity coefficient of a species either in a pure or mixed gases. The fugacity coefficient relations in terms of P and T, Volume-explicit and in terms of V and T, pressure- explicit respectively (Prausnitz et al.,1999).

$$\mathrm{RTln}\emptyset\mathrm{i} = \mathrm{RTln}\frac{\mathrm{f_i}}{\mathrm{y_i P}} = \int_0^{\mathrm{P}} \left[\left(\frac{\partial \mathrm{V}}{\partial \mathrm{n_i}} \right)_{\mathrm{T,P,n_{j\neq i}}} - \frac{\mathrm{RT}}{\mathrm{P}} \right] \mathrm{dP} \qquad (3.8)$$

$$\mathrm{RTln}\emptyset\mathrm{i} = \mathrm{RTln}\frac{\mathrm{f_i}}{\mathrm{y_i P}} = \int_{\mathrm{V}}^{\infty} \left[\left(\frac{\partial \mathrm{P}}{\partial \mathrm{n_i}} \right)_{\mathrm{T,V,n_{j\neq i}}} - \frac{\mathrm{RT}}{\mathrm{P}} \right] \mathrm{dV} - \mathrm{RTln z} \qquad (3.9)$$

Where z=pV/RT is the compressibility factor of mixture. Because most of the equations of state are pressure explicit, so equation (3.9) is the most convenient of the two.

3.2.2 Activity and Activity Coefficient

Activity Coefficient is an ideal approach to express the chemical potential in a real solution. The activity of component *i* at given temperature, pressure and composition is the ratio of fugacity at given temperature,pressure and composition to the fugacity of component *i* at standard state. Activity of a substance is the indication of how active a substance is relative to its standard state. It can be expressed as:

$$\alpha_i = \frac{f_i}{f_i^0} \qquad (3.10)$$

To measure the non ideality of the solution, the activity coefficient is introduced as:

$$\Upsilon_i = \frac{a_i}{x_i} \qquad (3.11)$$

3.2.3 Conventions for Activity Coefficient

The most common reference states are the pure component reference state (Raoult's law) and the infinite dilution reference state (Henry's law) as described below.

3.2.3.1 Symmetric Convention

This convention is often used when the components are in their pure states, both solutes and solvent at the system temperature and pressure, are liquids. The activity coefficient of each component then approaches unity as its mol fraction approaches unity. This convention leads to an ideal solution in the Raoult's law sense. It follows that:

$$\Upsilon_i \rightarrow 1 \text{ as } x_i \rightarrow 1$$

3.2.3.2 Asymmetric Convention

This convention is applied when the pure component is solid or gas at the system temperature and pressure. The reference state is defined as the infinite dilute state and activity coefficient is chosen to be unity as the mole fraction is approaches zero. This convention leads to an ideal dilute solution in the sence of Henry's law. The asymmetric activity coefficient r_i^* is the ratio of the actual activity coefficient and the activity coefficient at infinite dilution.

$$r_i^* = \frac{\gamma_i}{\gamma_i^\infty}$$

For solvent $\Upsilon_s \rightarrow 1$ as $x_s \rightarrow 1$

For ionic and moleculer solute $\Upsilon_s \rightarrow 1$ as $x_s \rightarrow 0$

3.3 Chemical and Phase Equilibria

3.3.1 Chemical Equilibrium

In the aqueous phase for the (AMP +CO_2+ H_2O) system, the following chemical equilibria are involved (Gabrielsen et. al., 2007)

Dissociation of water

$2H_2O \longleftrightarrow H_3O^+ + OH^-$ (R1)

Dissociation of CO_2 from gas phase to liquid phase

$CO_{2(g)} \xleftrightarrow{K1} CO_{2(l)}$

Hydrolysis of dissolve CO_2

$CO_2 + 2H_2O \xleftrightarrow{K2} H_3O^+ + HCO_3^{-1}$ (R2)

Dissociation of carbonate ion

$HCO^{-3} + H_2O \xleftrightarrow{K_3} H_3O^+ + CO_3^{-2}$ (R3)

Amine protonation

$AMP + H_2O \xleftrightarrow{K_4} AMPH^+ + OH^-$ (R4)

Carbamate formation of AMP (Ciftja, et al., 2010)

$AMP + CO_2 + H_2O \xleftrightarrow{K_5} AMPCOO^- + H3O^+$ (R5)

Chemical Equilibrium governs the extent of dissociation and reaction and so the distribution of species. The equilibrium condition stoichiometric formulation:

$$\sum_{i=1}^{n} \vartheta_i . \mu_i = 0 \qquad (3.12)$$

Where ϑ_i is stoichiometric coefficient of component i and μ_i is the chemical potential of component i. Traditionally, the chemical equilibrium is defined by the equilibrium constant , K.

$$K = \prod_{i=1}^{n} \alpha_i^{vi} = \prod_{i=1}^{n} \gamma_i^{vi} . x_i^{vi} \qquad (3.13)$$

Where γ_i is the activity coefficient and xi is liquid phase composition (Kohl & Nielsen, 1997).

The temperature dependency of the equilibrium constants defined in mole fraction scale and their sources are listed in table 3.1.

Table 3.1 Coefficients for the chemical coefficients for the chemical equilibrium constants used in the eNRTL model.

	A	B	*C*	*D*	T/K	Source
K_1	132.899	−13445.9	−22.4773	0	273 to 498	Edwards et al. (1978)
K_2	231.465	−12092.1	−36.7816	0	273 to 498	Edwards et al. (1978)
K_3	216.049	−12431.7	−35.4819	0	273 to 498	Edwards et al. (1978)
K_4	187.56±0.04	0	30.97±1.94	0.0373±0.0056	293 to 363	Kim et al. (2011)
K5	1265.837	-13948.1	-217.139	-.00212		Gupta et al,(2012)
ln K_i (mole fraction) = $a + b/T$(K) + C · ln T/(K) +DT(K) i = 1, 2, … , 4						

3.3.2 Phase Equlibrium

For a complete model of the AMP system, chemical equilibrium and vapor–liquid equilibrium must be solved simultaneously. The system is formulated as a standard VLE problem through the thermodynamic equilibrium criterion at given temperature and pressure.

$$\mu_i^{vap}(T,P,n) = \mu_i^{liq}(T,P,n) \qquad (3.14)$$

Where μ_i^{vap} and μ_i^{liq} are the chemical potentials of the species i in the vapor and liquid phase, respectively. The activity coefficient for species in the liquid phase were determined using the Electrolyte non-random two liquid (e-NRTL) framework and used in the phase equilibrium calculations. The Soave–Redlich–Kwong equation of state was used to calculate the gas phase properties **(Soave, 1972).** The equilibrium distribution of the volatile solute, CO_2, between the vapor and liquid was modeled based on Henry's law constant in water at system pressure and temperature as reference state. Because of the asymmetric reference state of CO_2, its phase equilibrium was calculated from:

$$\emptyset_{CO2} y_{CO2} P = \Upsilon_{CO2} x_{CO2} H_{CO2}^{\infty} \exp\left[\frac{v_{CO2}^{\infty}(P - P_{H2O}^{S})}{RT}\right] \qquad (3.15)$$

Where $\emptyset_{CO2}$ and y_{CO2} are the activity and the fugacity coefficients of CO2, respectively, P the total pressure, H_{CO2}^{∞} is the Henry's law constant of CO_2 in AMP, v_{CO2}^{∞} the infinite dilution partial molar volume of CO_2 and T(K) is the temperature. The reference states for water and amine were the pure components at system temperature and pressure. Thus pure solvent molecule follow the equation (3.16)

$$\emptyset_i^v y_i P = \Upsilon_i x_i P_i^0 \exp\left[\frac{v_i(P - P_i^0}{RT}\right] \qquad (3.16)$$

where yi and xi are concentration of species in the vapor and liquid phase, vi is the partial molar volume of component, P^0 is the vapor pressure, Υ_i is the activity coefficient of species i. The exponential correction term (Poynting Correction) takes into account that the liquid is at pressure P different from P_i^0. At low pressure the Pynting term can be disregarded. The coefficients for Henry's constant for CO2 in 3M AMP are taken from the experiment explained in section 3.3 are givrn in table A5 in Appendix.

3.4 Activity Coefficient Model

3.4.1 The NRTL Equation —Non-Electrolyte activity coefficient model

Wilson introduced the idea of local compositions for excess Gibbs energy**.** Renon and Prausnitz used the same concept in his derivation of NRTL (Non-random two liquid) equation. Renon's equation is applicable to partially miscible as well as completely miscible systems. The NRTL equation for the excess Gibbs energy is (Renon and Prausnitz., 1968)

$$\frac{G^E}{RT} = x_1 x_2 \left[\frac{\tau_{21} G_{21}}{x_1 + x_2 G_{21}} + \frac{\tau_{12} G_{12}}{x_2 + x_1 G_{12}}\right] \qquad (3.17)$$

where

$$\tau_{12} = \frac{g_{12} - g_{22}}{RT}$$

$$\tau_{21} = \frac{g_{21} - g_{11}}{RT}$$

$$G_{12} = \exp(-\alpha_{12}\,\tau_{12})$$

$$G_{21} = \exp(-\alpha_{12}\,\tau_{21})$$

Where g_{ij} is an energy parameter characteristic for i-j interaction and the parameter α_{12} is related to non-randomness in the mixture. Mixture is completely random for $\alpha_{12} = 0$

From equation (3.15) The activity coeffiecient are:

$$ln\gamma_1 = x_2^2 \left[\tau_{21}\left(\frac{G_{21}}{x_1 + x_2 G_{21}}\right)^2 + \frac{\tau_{21} G_{12}}{(x_2 + x_1 G_{12})^2}\right] \qquad (3.18)$$

$$ln\gamma_2 = x_1^2 \left[\tau_{12}\left(\frac{G_{12}}{x_2 + x_1 G_{12}}\right)^2 + \frac{\tau_{21} G_{21}}{(x_1 + x_2 G_{21})^2}\right] \qquad (3.19)$$

NRTL equation provides a good representation of experimental data for strongly non-ideal mixtures, and particularly for partially miscible systems. The activity coefficients were fitted in this work to the NRTL equation.

3.4.2 Electrolyte-NRTL—activity coefficient model

The NRTL model proposed by (Renon and Prausnitz.,1968) was originally non-electrolyte model. Chen and co-workers (Chen et al., 1986) developed the electrolyte NRTL model (e-NRTL), which is local composition model. It is assumed that, on a local scale, there are certain constraints on the composition of the mixture. For example, in the near vicinity of a cation, the likelihood of finding another cation is low. It may thus be assumed that there will be no ions of the same charge in the near vicinity of each other (like ion repulsion). In addition local electroneutrality must be satisfied. Chen et al.'s e-NRTL model was later extended to a segment based model, in which the molecules were split into interacting segments. This extension was primarily developed for predicting the behavior of macromolecules (e.g. micelles and polymer solutions (Chen et al., 2001) and (Chen et al., 2004). In the equations below, the excess Gibbs energy expression from the original e-NRTL model is given as in Chen and Evans (1986). In these equations *m*, *c* and *a* denote, respectively, molecular, cationic and anionic species. It should be noted that the excess Gibbs energy expression is the same for the original and the refined e-NRTL model. The major difference is of the activity coefficient expressions.

The activity coefficient, γi, for any species (ionic or molecular, solute or solvent) is calculated from the partial derivative of the excess Gibbs free energy with respect to mole number, ni.

$$\ln\gamma_i = \frac{1}{RT}\left[\frac{\partial(n_i G^{*E})}{\partial n_i}\right]_{T,P,n_{j\neq i}} \qquad i,j = m,c,a. \qquad (3.20)$$

The e-NRTL equation used in this work to calculate excess Gibbs free energy ($G*E$), is given by:

$$\frac{G^{*E}}{RT} = \frac{G^{*E,PDH}}{RT} + \frac{G^{*E,Born}}{RT} + \frac{G^{*E,Ic}}{RT} \qquad (3.21)$$

The model consists of one term that accounts for the short range forces ($G^{*E,lc}$), the e-NRTL term,one term that accounts for the long range forces ($G^{*E,PDH}$) and a Born term. The NRTL expression ($G^{*E,lc}$) for the short range interactions is given as follows:

$$\frac{G^{*E,lc}}{RT} = \sum_m X_m \frac{\sum_j X_j G_{jm}\tau_{jm}}{\sum_k X_k G_{km}} + \sum_c X_c \sum_{a'} \left(\frac{X_{a'}}{\sum_{a''} X_{a''}} \right) \frac{\sum_j X_j G_{jc,a'c}\tau_{jc,a'c}}{\sum_k X_k G_{kc,a'c}}$$
$$+ \sum_a X_a \sum_{c'} \left(\frac{X_{c'}}{\sum_{c''} X_{c''}} \right) \frac{\sum_j X_j G_{ja,c'a}\tau_{ja,c'a}}{\sum_k X_k G_{ka,c'a}}, \qquad (3.22)$$

Where

$$X_j = C_j x_j \quad j = m, c, a \qquad (3.23)$$

and

$$x_j = \frac{n_j}{\sum_i n_i} \quad j = m, c, a \qquad (3.24)$$

Xj is the effective mole fraction of species j and Cj=|zj| for ionic species and Cj = 1 for molecular species. 'zj 'is the charge number for the species j. G and τ are local binary quantities related to each other by non-randomness factor α; Gij=exp(−αijτij). where *j* and *k* can be any species. Some terms used in eq. 3.20 are explained here

Gjc,a'c=exp(-*αjc,a'c τjc,a'c*)

Gja,c'a=exp(-*αja,c'aτja,c'a*)

$$\tau_{cm} = -\frac{\ln G_{cm}}{\alpha_{cm}} \qquad (3.25)$$

$$\tau_{am} = -\frac{\ln G_{am}}{\alpha_{cm}} \qquad (3.26)$$

where *c*, *a*, and *m* represent cation, anion, and molecular species, respectively. *Xj* = *xj* · *Cj* (*Cj* = *zj* for ions and 1 for molecules), *x* is the mole fraction; *αij* is the non-randomness factor and *τij* is the binary energy interaction parameter. Non-randomness factors for molecule–molecule and molecule–electrolyte have been fixed at 0.2 as suggested by Chen and Even (Chen et al., 1986).

3.4.2.1 The Long Range Terms

The e-NRTL model consists of a long-range term and a short range term. The long-range or Coulombic interactions, so called the Pitzer Debye–Hückel term (*G∗E,PDH*) is used. (Pitzer.,1980)

$$\frac{G^{*E,PDH}}{RT} = -(\sum_k x_k)\left(\frac{1000}{M_s}\right)^{\frac{1}{2}}\left(\frac{4A_\phi I_x}{\rho}\right)\ln\left(1+\rho I_x^{\frac{1}{2}}\right) \qquad (3.27)$$

where Debye–Hückel parameter, *Aϕ*, and Ionic strength of solvent, *Ix*, are given by equations 3.28 and 3.29 respectively.

$$A_{\emptyset} = \frac{1}{3}\left(\frac{2\pi N_A d_s}{1000}\right)^{\frac{1}{2}}\left(\frac{Q_e^2}{\varepsilon_s kT}\right)^{\frac{3}{2}} \quad (3.28)$$

$$I_x = \frac{1}{2}\sum x_i z_i^2 \quad (3.29)$$

where *NA* is Avogadro's number, *k* is the Boltzman constant, *Qe* is electron charge, *ds* is the density of the solvent and *z* is the charge number of ion. The reference state for ionic species in Pitzer-Debye-Huckel equation is the the infinite dilution in the mixed solvent and the reference state for short range term is the infinitely diluted aqueous solution, so Born term is added. This term is means to correct for the difference between the dielectric constant of water and the mixed solvent (Born, 1920; Harned and Owen., 1958; Thomsen., 2006)

$$\frac{G^{*E,Born}}{RT} = \left(\frac{Q_e^2}{2kT}\right)\left(\frac{1}{\varepsilon_s} - \frac{1}{\varepsilon_e}\right)\sum_i \frac{x_i z_i^2}{r_i} 10^{-2} \quad (3.30)$$

where εs and εw represent the dielectric constant of the mixed solvent and pure water, respectively. The dielectric constant of water and AMP is given in table 3.2.(Sukanta et al., 2011)

Table 3.2 Dielectric constants of AMP and water

Species	***a₁***	***b₁***
H_2O	78.65	31989
AMP	21.9957	8992.68
ε = a1 + b1/T (K) [1/T (K) – 1/298.15]		

From the model developed above, it can be seen that several pure component and binary parameters and properties are involved. The pure component parameters such as critical constants, acentric factor, compressibility factor and Brelvi–O'Connell parameter, Antoine equation constants for the vapour pressure of molecular species are taken from DIPPR data base and summarized in table 3.3 and 3.4

Table 3.3 Pure component physical properties for VLE model

Properties	H_2O	CO_2	AMP
T_c/K	647.30	304.20	619.818
P_c/kPa	22,048	7376.0	4862.97
$V_c/(m^3 \cdot kmol^{-1})$	0.0559	0.0939	0.29650
Acentric factor (ω)	0.3440	0.2250	0.74259
Racket Z_{RA}	0.2432	0.2736	0.26720
Brelvi–O'Connell parameter	0.0464	0.0939	

Table 3.4 Antonic equation coefficient of molecular species

Components	H_2O	AMP	CO_2	Ions
A	72.55	20.0032	72.82912	1.00E+20
B	7206.7	2859.28	3403.28	0
C	0	159.672	0	0
D	0	0	9.49E-03	0
E	7.1385	0	8.56034	0
F	4.05E-06	0	2.91E-16	0
G	2	0	6	0
ln(p0/Pa) = A + B/T(K)+C + D(T/K) +Eln(T/K) + F(T/K)				

Chapter 4

Results and Discussion

4.1 Experimental results and discussion

This study report presents VLE (vapor liquid equilibria) of the AMP-CO_2-H_2O and PZ-CO_2-H_2O systems. The results for vapor liquid equilibrium were obtained over aqueous AMP solutions with different concentrations (3M/26.84 %wt), 0.1M/0.89 %wt and 1M/9 %wt) and 1.5M PZ by both low (atmospheric) pressure and high-pressure equipments, are presented in Appendix table A1, A2, A3 and A4 . Low pressure (atmospheric) equipment was used to collect the data at 40 °C, 60 °C and 80 °C and high pressure equipment was used to collect the data at 80°C 100 °C and 120 °C.

Atmospheric pressure equipment cannot be operated at temperatures above 80° C. Partial pressures of CO_2 range between 0.0162 to 1001.9 kPa for AMP-CO_2-H_2O system and 0.03 to 973.9kPa for Pz-CO_2-H_2O system and CO_2 loading is confined between 0.067 and 0.9786 (mol of CO_2/mol of AMP) and 0.05 to 0.8987 (mole of CO_2/mole of PZ) respectively. Graphically representation of data generated with both the apparatuses is shown in figures 4(a), 4(b), 4(c) and 4(d). In the graphical representation it should be noted that at 40, 60 and 80^{0}C, it is a partial pressure of CO_2 and at 100 and 120^{0}C, it is the total pressure.

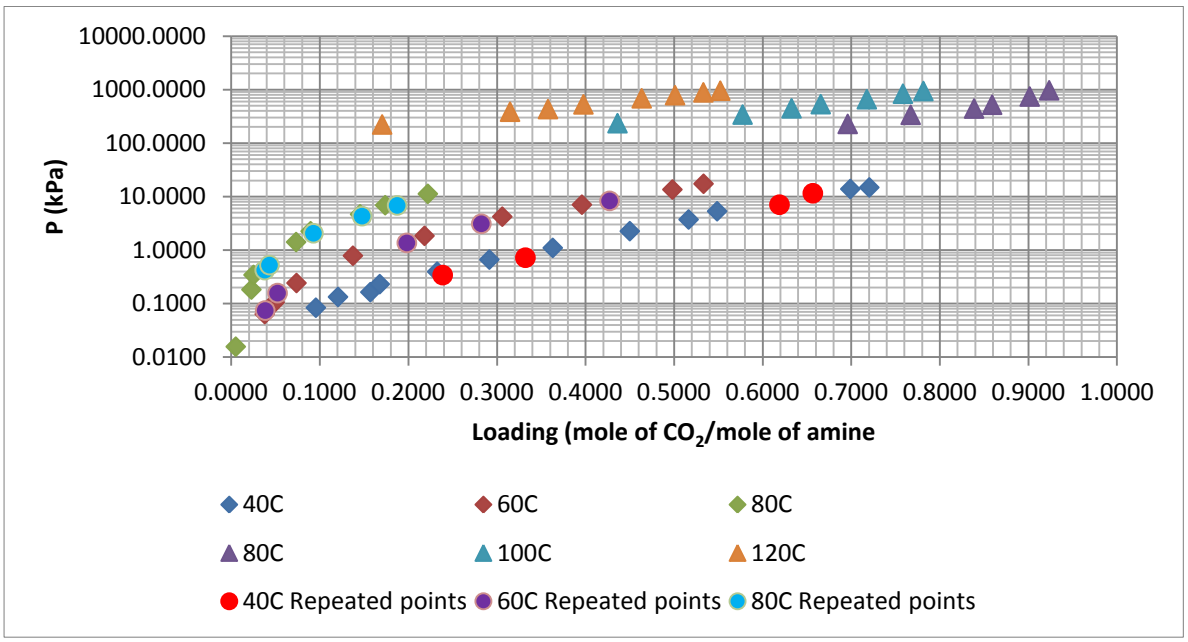

Figure 4(a) Experimental VLE data of 3M AMP

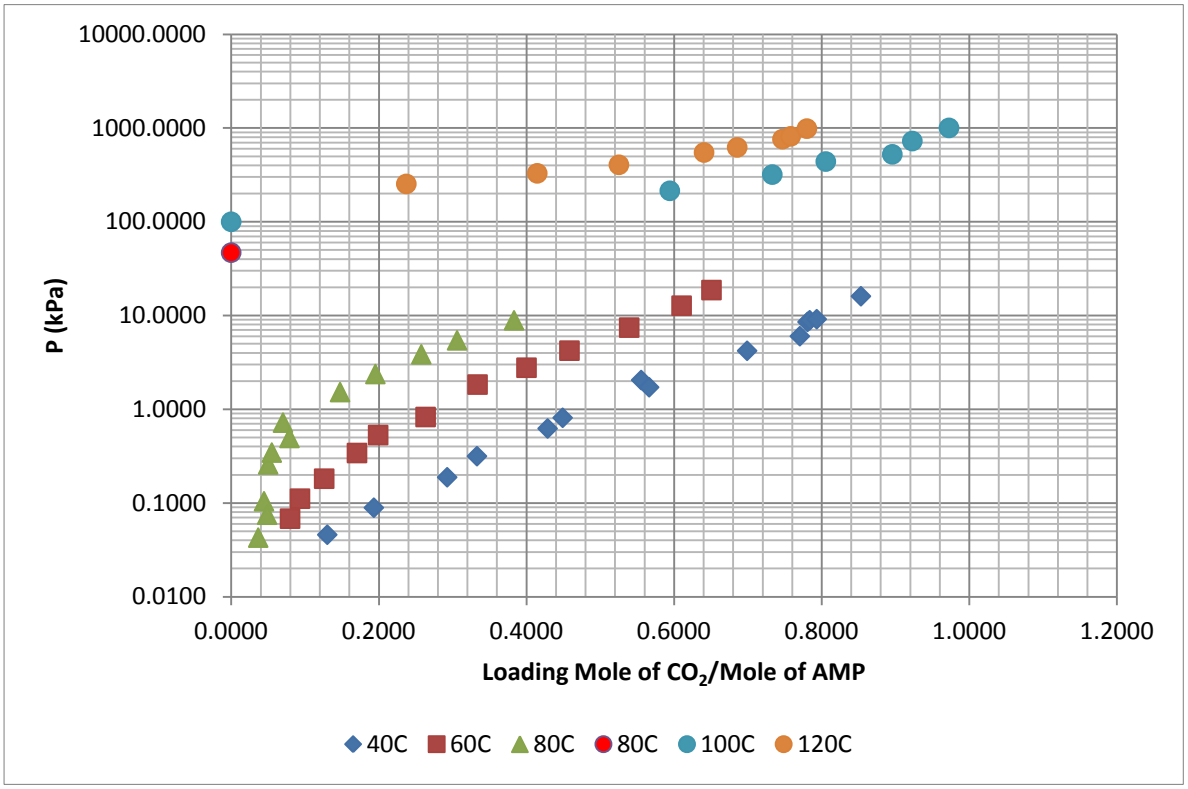

Figure 4(b) Experimental VLE data of 1M AMP

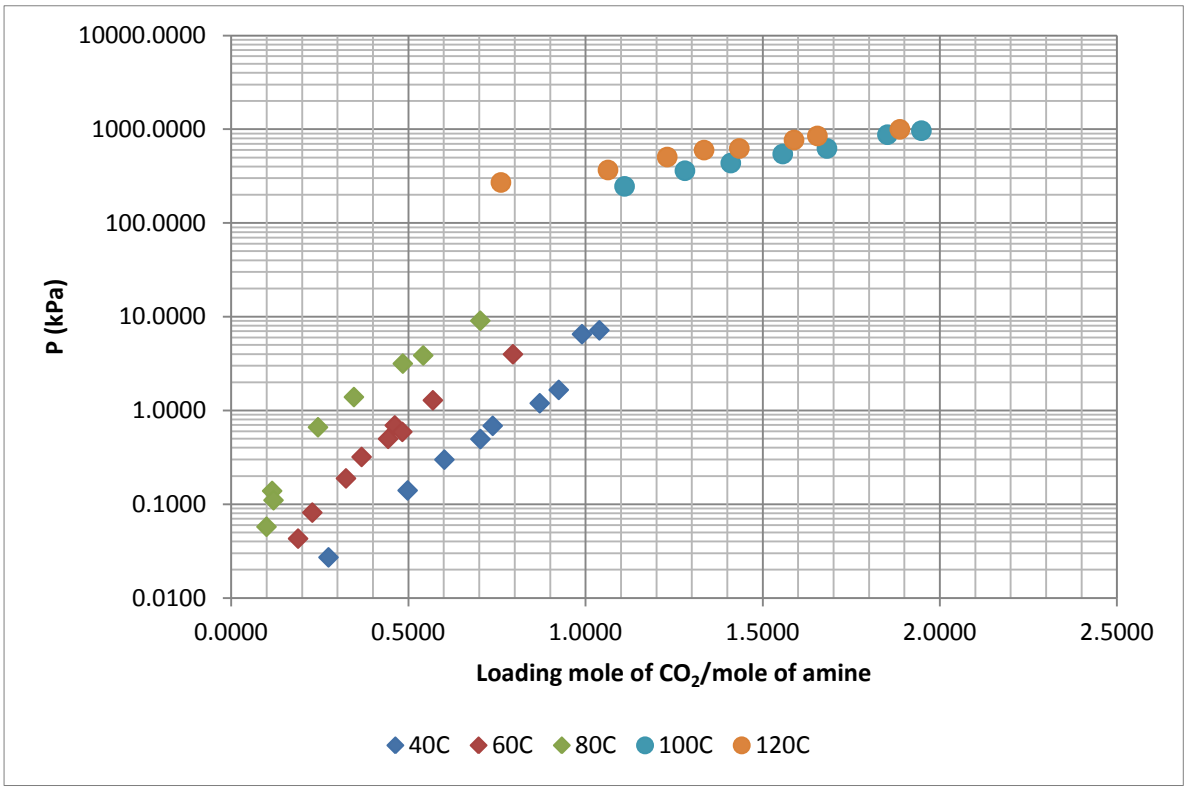

Figure 4(c) Experimental VLE data of 0.1M AMP

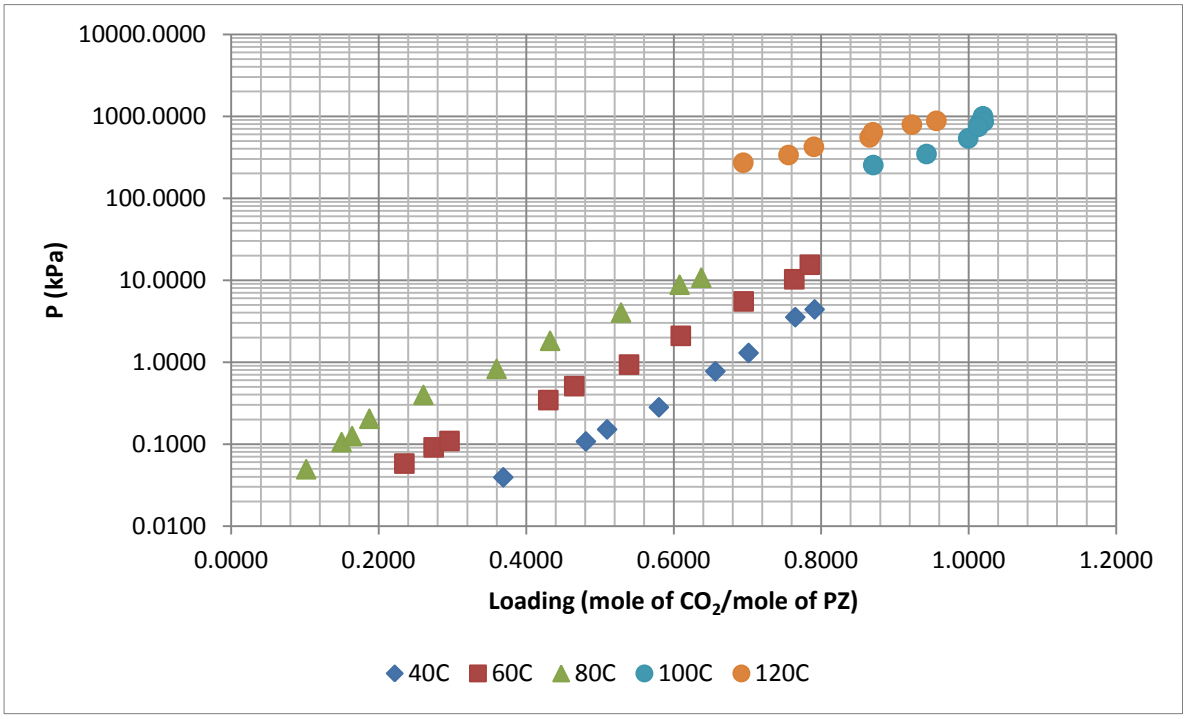

Figure 4(d) Experimental VLE data of 1.5M PZ

4.1.1 Reproducibility of the data

For the validation of the measurement procedure and to check the quality of data, some data points were reproduced by low pressure equipment at temperature 40,60 and 80 ^{0}C. It is evident from the figure 4(a) that the reproduced data is remarkable in terms of both trends and reproducibility. The present data was also compared with the literature data to check the quality of the data. From the figure 4(f), it can be seen that the measurement of this work agrees well with the data reported by yang et al., 2010 at 40^{0}C. It is observed from the figures 4(a-c) that the partial pressure of CO_2 is small at low CO_2 loading. The CO_2 partial pressure increases rapidly at high gas loading. When in the liquid phase AMP is almost spent by chemical reaction, CO_2 can no longer be predominantly absorbed chemically but has to be absorbed by dissolution. Due to this major role of physical absorption at high gas loading, the effect of pressure and temperature on CO_2 loading is relatively less pronounced at high pressure and the experimental data at different temperature are very close to each other at high pressure as observed in 4(b) and 4(c).

4.1.2 Concentration dependency of CO_2 Partial Pressure for AMP-CO_2-H_2O System

Figure 4(e) demonstrates the influence of AMP concentration on CO_2 partial pressure. It is observed that the CO_2 partial pressure increases with AMP concentration at constant temperature and at

particular CO_2 loading. Kundu et al., (2003) and Sukanta et al., (2011), have also reported similar observations.

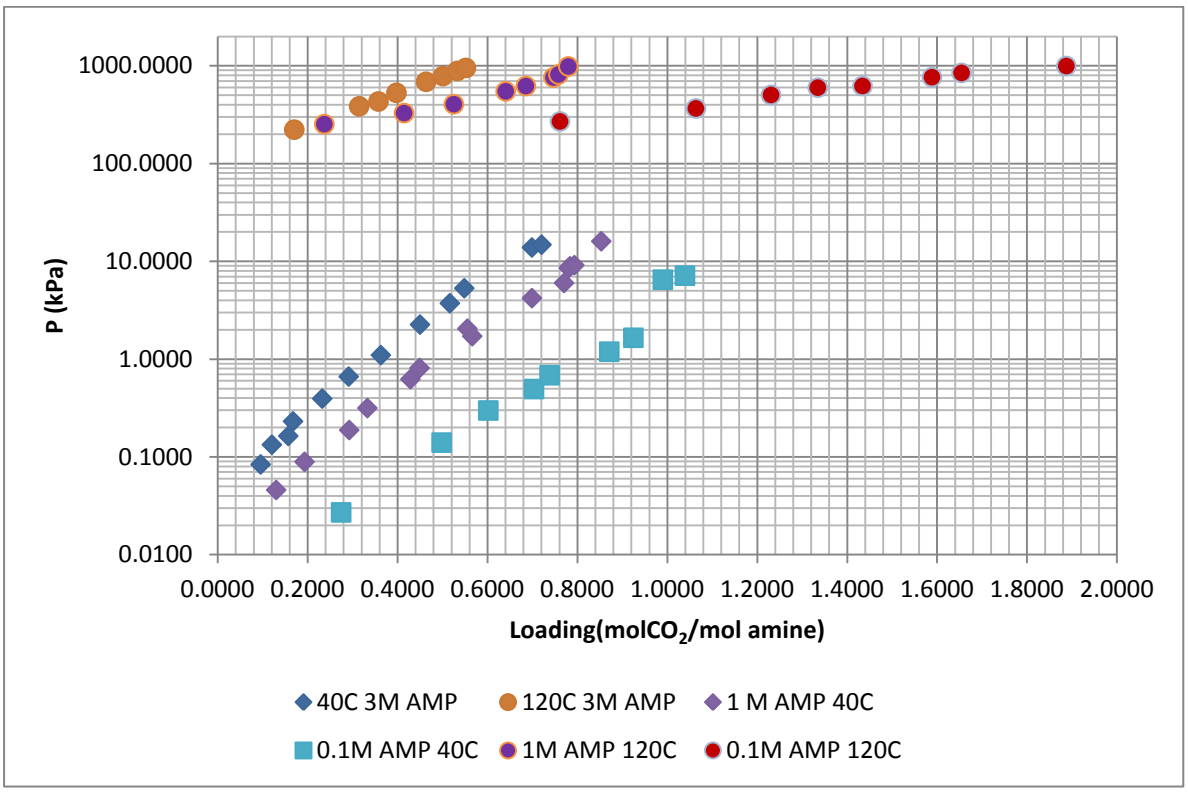

Figure 4(e) Concentration dependency of CO_2 Partial pressure for AMP+CO_2+H_2O system.

The expression for the dependency of CO_2 partial pressure on amine concentration can be derived using simplified explicit method as, (Astaria et al., 1983)

$$AMP + CO_2 \xleftrightarrow{K_{eq}} AMPH^{+} + HCO_3^{-1} \qquad (4.1)$$

$$Keq = \frac{[HCO_3^-][AMPH^+]}{P_{CO2}\,[AMP]} \qquad (4.2)$$

$$Keq = \frac{[m\alpha]^2}{P_{CO2}\,[m[1-\alpha]} \qquad (4.3)$$

$$P_{CO2} = \frac{m[\alpha]^2}{Keq\,[[1-\alpha]} \qquad (4.4)$$

In view of the very low carbamate stability constant of the sterically hindered amine (Sartori and Savage, 1983), the only reaction of importance between CO_2 and AMP is suggested to be the formation of bicarbonate ions. Hence, bicarbonate ions may be present in the solution in much larger amounts than the carbamate ions. Equation (4.4) shows the CO_2 partial pressure is dependent on amine concentration due to bicarbonate formation. This concentration dependency of CO_2 partial for the AMP system can also be shown as determined experimentally.

Figure 4(e) also shows that an increase in concentration of AMP higher then 0.1M could give some advantages in terms term of CO_2 removed during absorption up to the rich loading (mole of CO_2/mole of amine) at 40 ^{0}C and desorption at 120 ^{0}C down to the lean loading (mole of CO_2/mole of amine). The figure 4(e) shows a significant change in equilibrium partial pressure for 3M AMP as compare to 1M AMP and 0.1M AMP representing more CO_2 in gas phase for 3M AMP.

The ratio P^*_{CO2}/P_{H2O} is higher in 3M AMP implying lower stripping steam requirement in 3M AMP system. This indicates that using an increased AMP concentration may have potential for more energy efficient CO_2 removal. The use of less steam requirement for regeneration results in cutting down the reboiler duty.

4.1.3 Comparison with literature

Referring to figure 4(f), this work is compared with the literature data available. This work at 40 °C is compared with work done by (Yang et al., 2010) and (Robert and Mather, 1988). The data points of this work falling at lower loading and lacking of data at high loading. The CO_2 partial pressure of this work is bit higher but overall it is in good agreement with the literature data points. There is not enough data available in literature at high (stripping) temperature to compare with this work.

The comparison of this work with the data of (Tontiwachwuthikul et al., 1991) at 40, 60 and 80^{o}C shows that present work has slightly higher values of partial pressures of CO_2. The difference may be attributed to difference in their VLE measurement equipment and procedure or may the difference of analysis techniques for CO_2 measurement. This work has advantage of having lowest values of loading and partial pressures ever obtained but it is lacking data on higher loading.

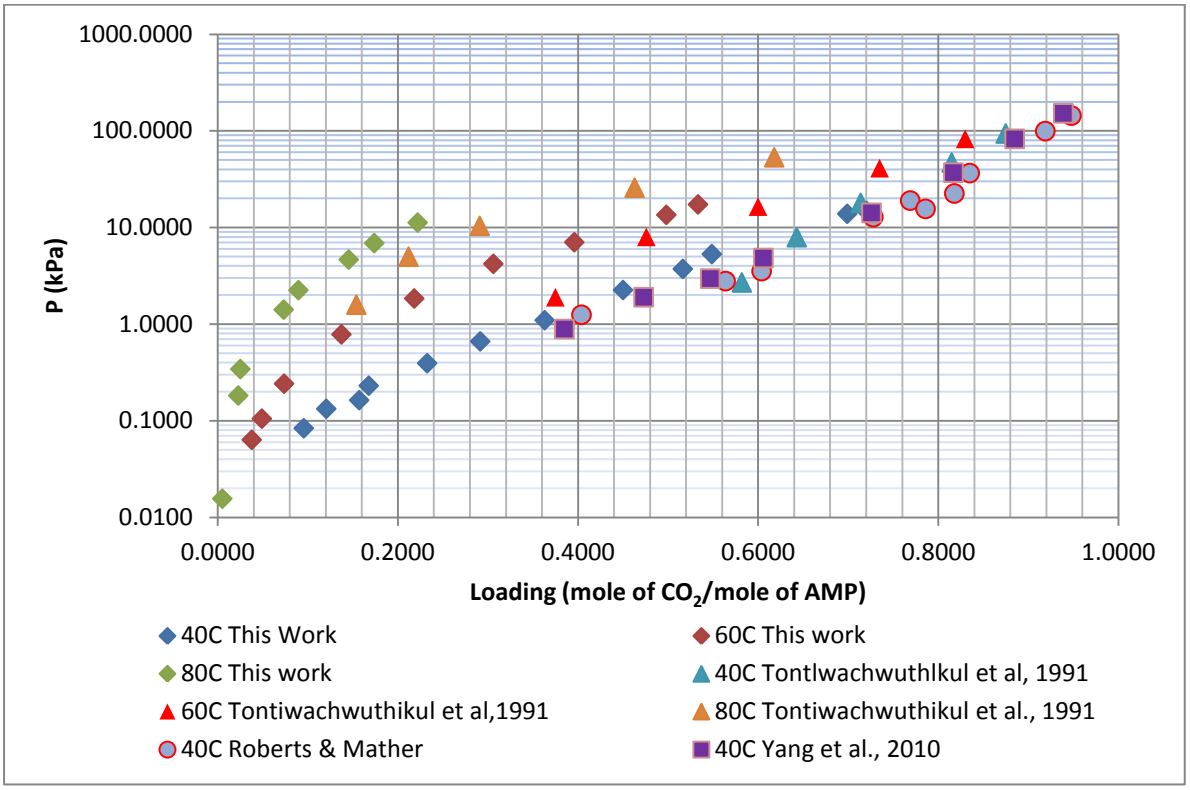

Figure 4(f) Comparison of 3M AMP with Literature

4.2 Modeling Results and discussion

The binary system consists of H_2O and AMP. The degree of dissociation of such a system is very low and presence of ions can be neglected. In the model parameters regression for more complex amine-CO_2-H_2O system, it is reasonable to determine first the binary interaction parameters from the experiments on the binary systems. The total and partial pressure experimental data could be used in the regression of binary interactions parameters for two component systems. The activity coefficient (experimentally) for AMP-H_2O system was calculated using equation (3.16) and fitted to the NRTL equation described in section 3.4.1. The NRTL parameters can be used as molecule – molecule binary interaction parameters in the e-NRTL model of Chen (Chen et al., 1986).

4.2.1 Binary System (AMP-H_2O)

4.2.1.1 Binary interaction parameters Regression

Binary interaction parameters for molecule-molecule were regressed using the binary VLE data from Hartono (Hartono et al., 2012) and excess enthalpy data from (Mathonat et al., (1997). Non-randomness factors for molecule–molecule has been fixed at 0.2 as suggested by Chen (Chen et al.,1986). Moreover, Chen and Evans (1986) found that ion pair-ion pair parameters could usually be

set to zero without significantly affecting representation of VLE data.A temperature dependent form of binary parameters was used for the NRTL equation as:

$$\tau_{12} = a_{12} + \frac{b_{12}}{T(K)}$$

$$\tau_{21} = a_{21} + \frac{b_{21}}{T(K)}$$

$$\alpha_{12} = \alpha_{21} = 0.2$$

The regression analysis was performed through the optimization method PSO (lbest) using the MATLAB based parameter estimation tool, *Modfit* (Diego Di. D Pinto and Juliana Monteiro PhD students at NTNU). The objective function used to minimize the error is given as:

$$AARD\% = \frac{1}{NP}\sum\left(\frac{P^{exp} - P^{calc}}{P^{exp}}\right).100 + \frac{1}{NP}\sum\left(\frac{H^{exp} - H^{calc}}{H^{exp}}\right).100 \qquad (4.5)$$

Regressed binary interaction parameters for AMP+H_2O are given in the table 4.1

Table 4.1 Regressed Binary NRTL parameters and AARD%

Parameters	a_{12}	a_{21}	b_{12}	b_{21}
H_2O-AMP	3.1621	-0.018502	100.7354	-667.6518
	P_{total}	Heat Excess		
AARD%	0.009	5.7		

4.2.2.1 The AMP-H_2O Subsystem

Binary interaction parameters (see table 4.1) for AMP-H_2O system were regressed using the binary VLE data for this system from Hartono et al., 2012. The NRTL Model prediction results for total pressure are shown in the fig 4.1(a-c) while fig 4.2(a-c) shows the results for activity coefficients of AMP solution.

The figures 4.1(a-c) give the isothermal dependence of total pressure on liquid and vapor phase compositions. It can be seen from the figure that total pressure decreases as liquid and vapor

concentration increases. The NRTL model seems to give an excellent agreement with the experimental data for total pressure within an AARD of 0.09% (see fig 4.1d)

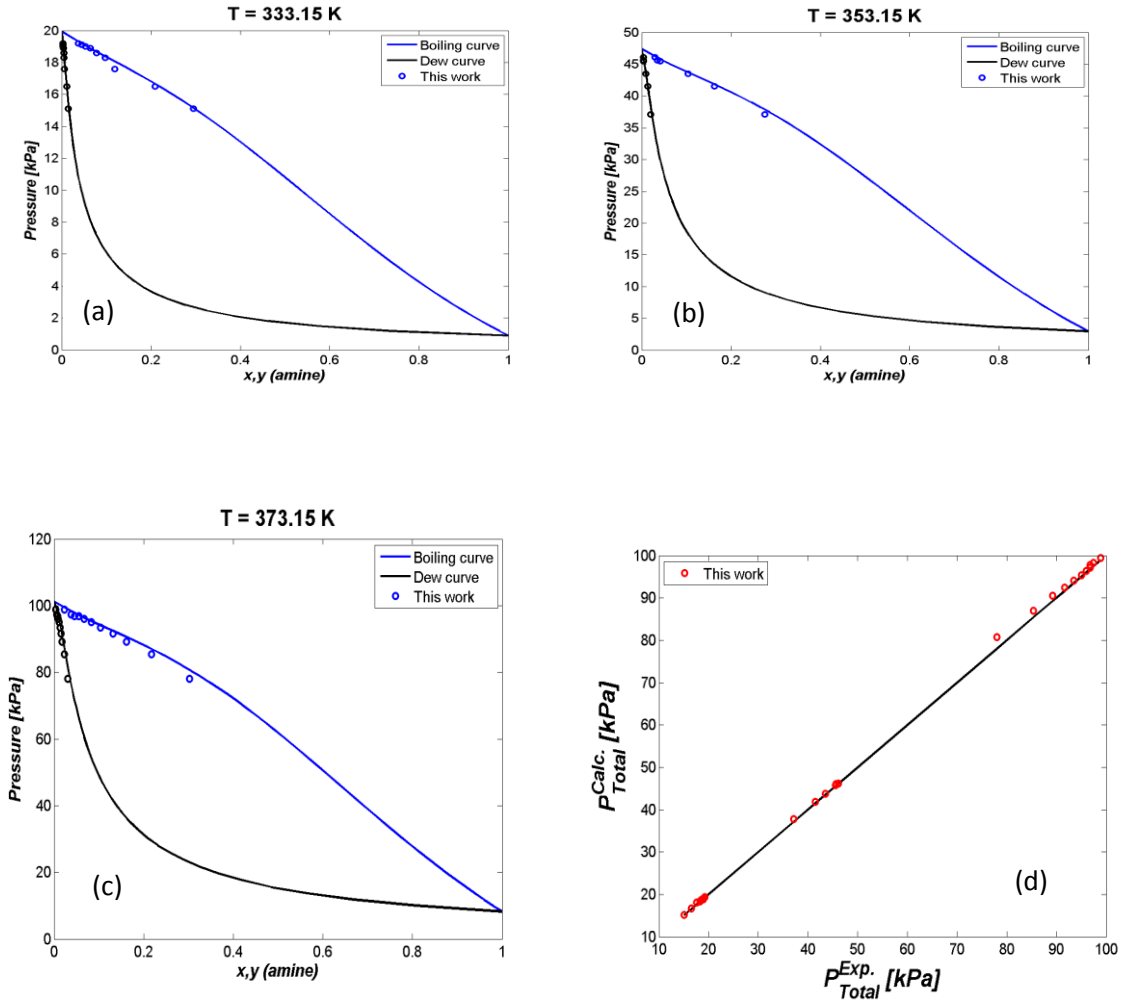

Figure 4.1: (a- c) Pxy diagram for binary AMP-water system. –, liquid phase, xAMP; –, vapor phase, yAMP, (d) Parity plot between experimental and model predicted total pressure; Experimental data points: Hartono et al., 2012. Solids lines NRTL model

The measured activity coefficients as a function of liquid concentrations at temperatures 60, 80 and 100 ^{0}C are shown in the fig.4.2 (a-c) respectively. It is seen that activity coefficients of AMP at temperature 60, 80 and 100 ^{0}C are higher than one (1) for liquid concentration lower than 0.2.

The temperature has different effect on the activity coefficient of different species in solution. The activity coefficient of water is almost constant at all temperature while the activity coefficient of AMP slightly increases with temperature as shown in figure 4.2 (a-c). The NRTL model predicts well the experimental activity coefficient at low liquid and vapor phase concentration of AMP but slightly deviates at concentration above 0.2.

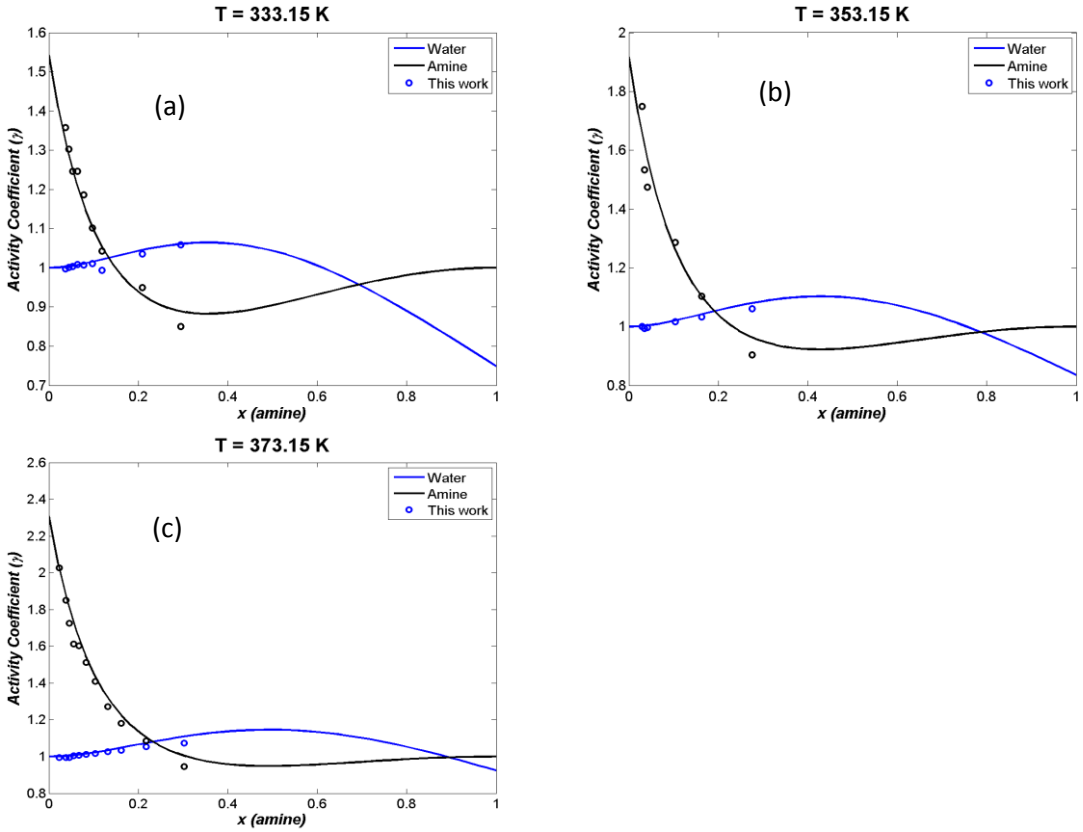

Figure 4.2(a-c) Activity coefficient of AMP AMP-H_2O system; data points Hartono et al., 2012; solids lines NRTL model

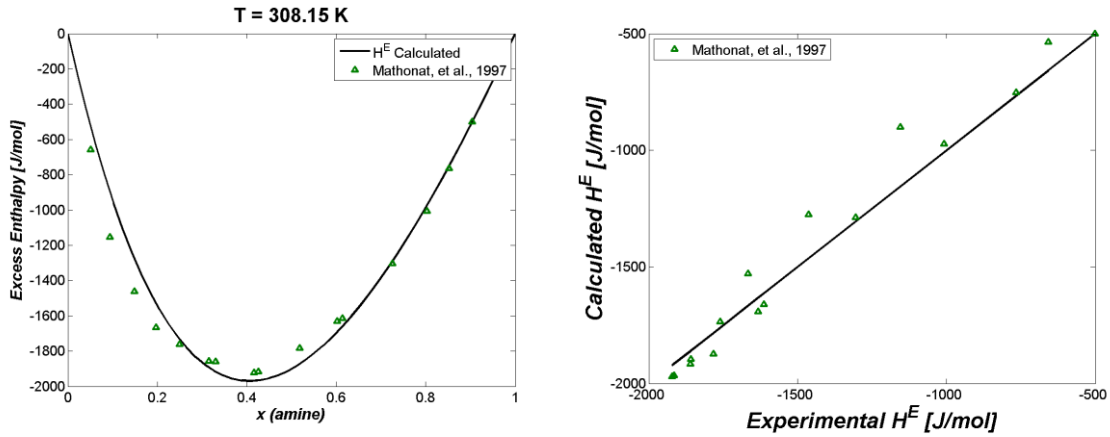

Figure 4.3: (a) Excess enthalpy H2O-AMP ; experimental data points: Mathonat et al., (1997 solid lines NRTL model (left) and Parity plot of excess enthalpy(right)

Figure 4.3(a) shows the results for model predictions of excess enthalpy of AMP compared to data from Mathonat et al. (1997). The model also shows a good fit to the excess enthalpy data. The experimental data and model predictions are in very good agreement at liquid phase amine concentration greater than 0.6. The model represents under predictions between liquid phase

concentration of 0.3 and 0.6 while over predictions at liquid phase concentration less than 0.3. The overall AARD is 5.7% which is a reasonable value.

4.2.2 Ternary System (Case 1)

4.2.2.1 Ternary interaction parameters regression without solubility data

Ternary interaction parameters for AMP-CO_2-H_2O system were regressed using the experimental CO_2 partial pressure (PCO_2), and total pressure (Pt) from this work for (26.84, 9 and 0.89)wt % AMP (table A1, A2 and A3 in Appendix). No literature data was used for parameters regression. Non-randomness factors molecule–electrolyte have been fixed at 0.2 as suggested by Chen (Chen et al., 1986). Temperature dependent form of ternary parameters was used in e-NRTL equation as:

$$\tau_{m,ca} = a_{m,ca} + \frac{b_{m,ca}}{T(K)}$$

$$\tau_{ca,m} = a_{ca,m} + \frac{b_{ca,m}}{T(K)}$$

$$a_{H2O,ca} = 0.2$$

$$a_{ca,CO2/Am} = 0.1$$

The regression analysis was performed through the optimization method PSO (lbest) using the MATLAB based parameter estimation tool, *Modfit* (Diego Di. D Pinto and Juliana Monteiro PhD students at NTNU). The objective function used to minimize the error is given as:

$$AARD\% = \frac{1}{NP}\sum\left(\frac{{P_{CO_2}}^{exp} - {P_{CO_2}}^{calc}}{{P_{CO_2}}^{exp}}\right).100 + \frac{1}{NP}\sum\left(\frac{{P_{total}}^{exp} - {P_{total}}^{calc}}{{P_{total}}^{exp}}\right).100 \qquad (4.6)$$

Regressed ternary interaction parameters for AMP-CO_2-H_2O system are given in the table 4.2. The parameters are set equal to default values used in Aspen Plus (2008): $\tau_{H2O,ca}$= 8, $\tau_{ca,H2O}$=-4, $\tau_{CO2/amine,ca}$=15 and $\tau_{ca,CO2/amine}$ = -8. The molecule-ion pair and ion pair-molecule parameters are normally insignificant and assigned a default value of zero (see table 4.2).

w

Table 4.2 Regressed ternary e-NRTL parameters without physical solubility data

Legend									
1	H_2O	4	H_3O^+	7	HCO_3^-				
2	CO_2	5	$AMPH^+$	8	CO_3^{-2}				
3	AMP	6	OH-	9	AMPCO2-				
	a (-)		**b (K)**	**Source**		**a (-)**		**b (K)**	**Source**
$a_{1,4-6}$	8	$b_{1,4-6}$	0	Default	$a_{4-6,1}$	-4	$b_{4-6,1}$	0	Default
$a_{1,4-7}$	8	$b_{1,4-7}$	0	Default	$a_{4-6,2}$	-8	$b_{4-6,2}$	0	Default
$a_{1,4-8}$	8	$b_{1,4-8}$	0	Default	$a_{4-6,3}$	3.625092	$b_{4-6,3}$	-47.5569	Regressed
$a_{1,4-9}$	-3.34996	$b_{1,4-9}$	346.6286	Regressed	$a_{4-7,1}$	-4	$b_{4-7,1}$	0	Default
$a_{1,5-6}$	-7.36708	$b_{1,5-6}$	-362.946	Regressed	$a_{4-7,2}$	-8	$b_{4-7,2}$	0	Default
$a_{1,5-7}$	-3.50257	$b_{1,5-7}$	392.8887	Regressed	$a_{4-7,3}$	-6.55441	$b_{4-7,3}$	-17.8669	Regressed
$a_{1,5-8}$	-5.2207	$b_{1,5-8}$	117.0461	Regressed	$a_{4-8,1}$	-4	$b_{4-8,1}$	0	Regressed
$a_{1,5-9}$	-7.31313	$b_{1,5-9}$	-225.095	Regressed	$a_{4-8,2}$	-8	$b_{4-8,2}$	0	Regressed
$a_{2,4-6}$	15	$b_{2,4-6}$	0	Default	$a_{4-8,3}$	-3.00741	$b_{4-8,3}$	266.5487	Regressed
$a_{2,4-7}$	15	$b_{2,4-7}$	0	Default	$a_{4-9,1}$	-7.35645	$b_{4-9,1}$	944.903	Regressed
$a_{2,4-8}$	15	$b_{2,4-8}$	0	Default	$a_{4-9,2}$	6.473368	$b_{4-9,2}$	698.2679	Regressed
$a_{2,4-9}$	3.710554	$b_{2,4-9}$	592.0001	Regressed	$a_{4-9,3}$	7.402164	$b_{4-9,3}$	-393.996	Regressed
$a_{2,5-6}$	0.562666	$b_{2,5-6}$	66.38358	Regressed	$a_{5-6,1}$	4.391426	$b_{5-6,1}$	618.0047	Regressed
$a_{2,5-7}$	2.312988	$b_{2,5-7}$	800.9186	Regressed	$a_{5-6,2}$	-7.8029	$b_{5-6,2}$	-141.462	Regressed
$a_{2,5-8}$	7.950687	$b_{2,5-8}$	-369.563	Regressed	$a_{5-6,3}$	-3.2704	$b_{5-6,3}$	219.8246	Regressed
$a_{2,5-9}$	2.029114	$b_{2,5-9}$	-248.34	Regressed	$a_{5-7,1}$	-2.05124	$b_{5-7,1}$	310.9437	Regressed
$a_{3,4-6}$	-0.32015	$b_{3,4-6}$	19.4999	Regressed	$a_{5-7,2}$	0.99206	$b_{5-7,2}$	489.3538	Regressed
$a_{3,4-7}$	2.565584	$b_{3,4-7}$	-66.0315	Regressed	$a_{5-7,3}$	-6.33007	$b_{5-7,3}$	522.0313	Regressed
$a_{3,4-8}$	4.101761	$b_{3,4-8}$	538.2949	Regressed	$a_{5-8,1}$	-1.65362	$b_{5-8,1}$	32.22483	Regressed
$a_{3,4-9}$	-5.08478	$b_{3,4-9}$	281.1706	Regressed	$a_{5-8,2}$	-2.60699	$b_{5-8,2}$	513.2948	Regressed
$a_{3,5-6}$	-1.2467	$b_{3,5-6}$	467.181	Regressed	$a_{5-8,3}$	4.67383	$b_{5-8,3}$	471.9254	Regressed
$a_{3,5-7}$	1.85217	$b_{3,5-7}$	498.867	Regressed	$a_{5-9,1}$	2.557528	$b_{5-9,1}$	-483.239	Regressed
$a_{3,5-8}$	-3.08683	$b_{3,5-8}$	468.689	Regressed	$a_{5-9,2}$	-2.20804	$b_{5-9,2}$	229.5191	Regressed
$a_{3,5-9}$	-0.49357	$b_{3,5-9}$	-180.144	Regressed	$a_{5-9,3}$	-10.6877	$b_{5-9,3}$	651.1307	Regressed

4.2.2.2 Full model prediction AMP-CO_2-H_2O

The regressed binary and ternary interaction parameters are given in table 4.1 and 4.2 respectively. Model calculations and experimental CO_2 partial pressures, and total pressure from this work as a function of loading and temperature are shown in figure 4.4 and 4.5

From the figures below it can be seen that the model predictions for CO_2 partial pressure are in good agreement with all data points. The model also predicts well the total pressure at 100 and 120^{0}C but it under-predicts the total pressure at 80^{0}C beyond the loading 0.85 mole of CO_2/mole of amine as shown by the figure 4.5.

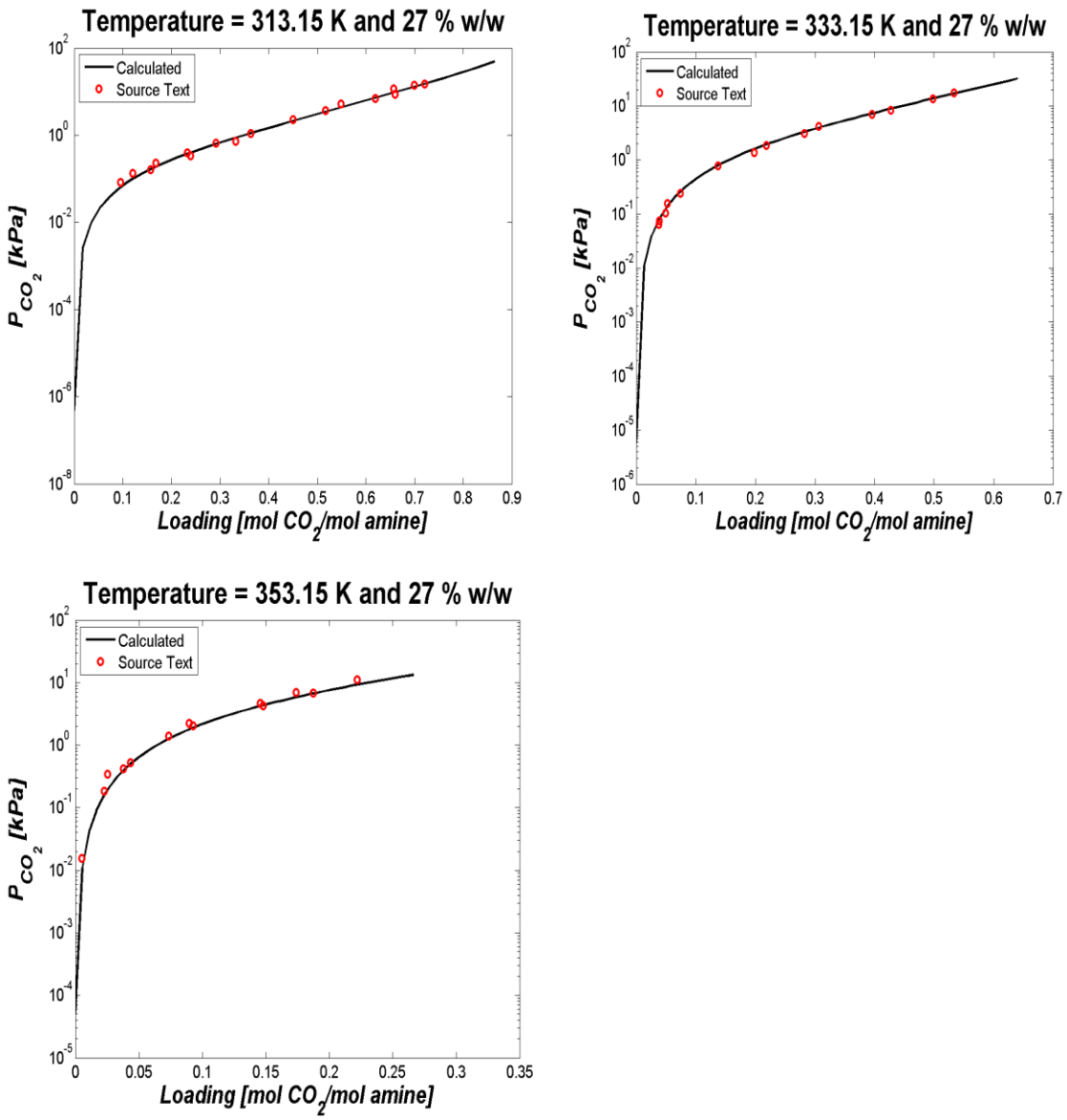

Figure 4.4 e-NRTL representation of CO_2 partial pressure over AMP-CO_2-H_2O system: experimental data: this work; solid lines e-NRTL mode

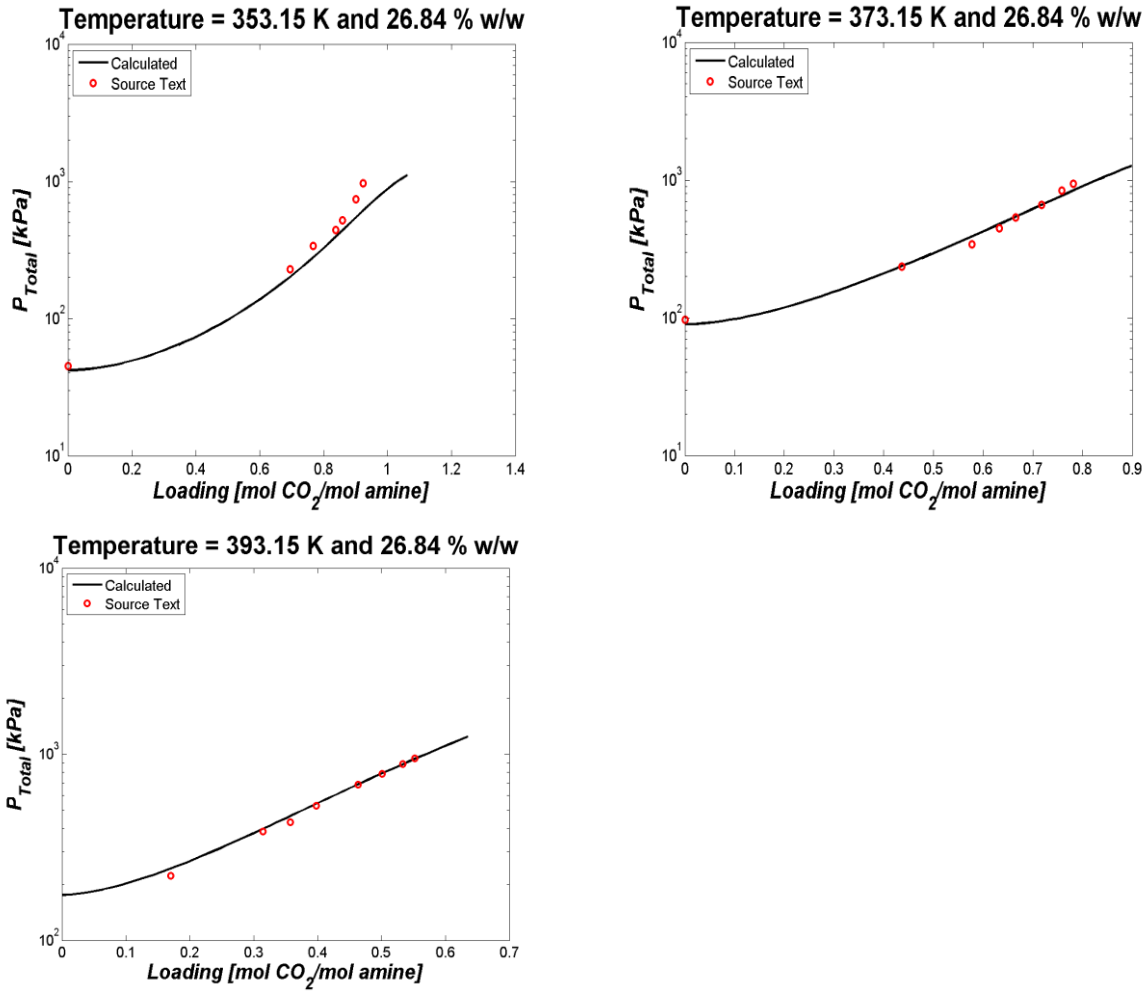

Figure 4.5 e-NRTL representation of total pressure over AMP-CO_2-H_2O system: experimental data: this work; solid lines e-NRTL model

The e- NRTL model predictions of CO_2 partial pressure and total pressure for 9 and 1 wt% AMP are compared by this experimental work in fig 4.6 - 4.9. It can be seen that the model predictions of CO_2 partial pressure and total pressure are in good agreement at loading below 0.8 mole of CO_2/mole of amine over all temperature ranges. For loading higher then 0.8mole of CO_2/mole of amine the model over-predict the CO_2 partial pressure (fig. 4.8) while under-predicts the total pressure (4.7).

Total 93 data points for CO_2 partial pressure and 53 data points for total pressure were used for model prediction. Model is predicting most of the data points of CO_2 partial pressure as well as total pressure. The overall AARD for CO_2 partial pressure and total pressure is 19.82% and 9.42% respectively which is reasonably good value. This deviation may be attributed to the reasons that the error in the estimation of interaction parameters or parameters fitting. The experimental data may have some error as well. The interactions parameters were regressed using only this experimental data. Unfortunately, no high pressure VLE data is available in literature to figure out the precision of experimental high pressure VLE data.

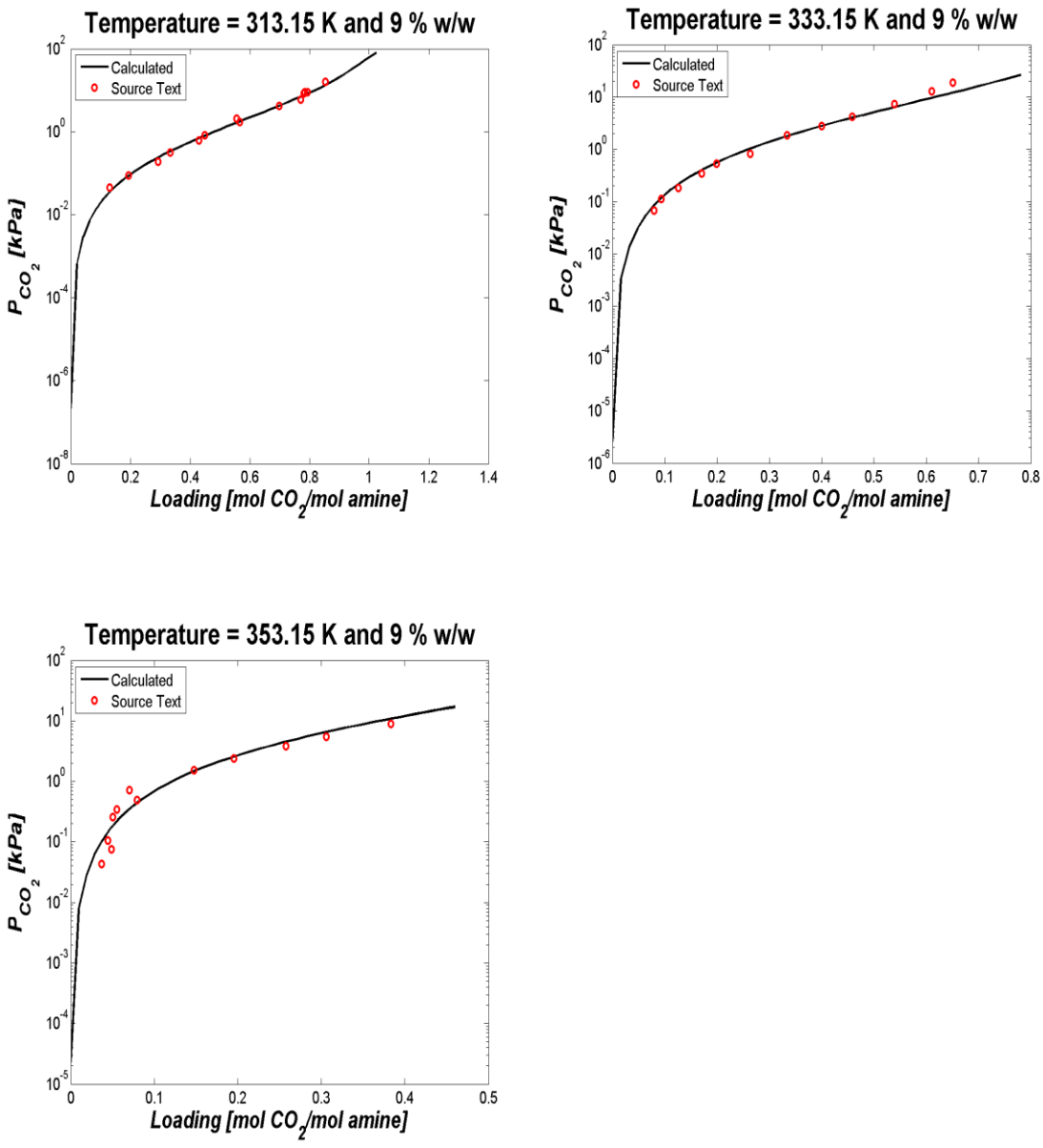

Figure 4.6 e-NRTL representation of CO_2 partial pressure over AMP-CO_2-H_2O system: experimental data: this work; solid lines e-NRTL mode

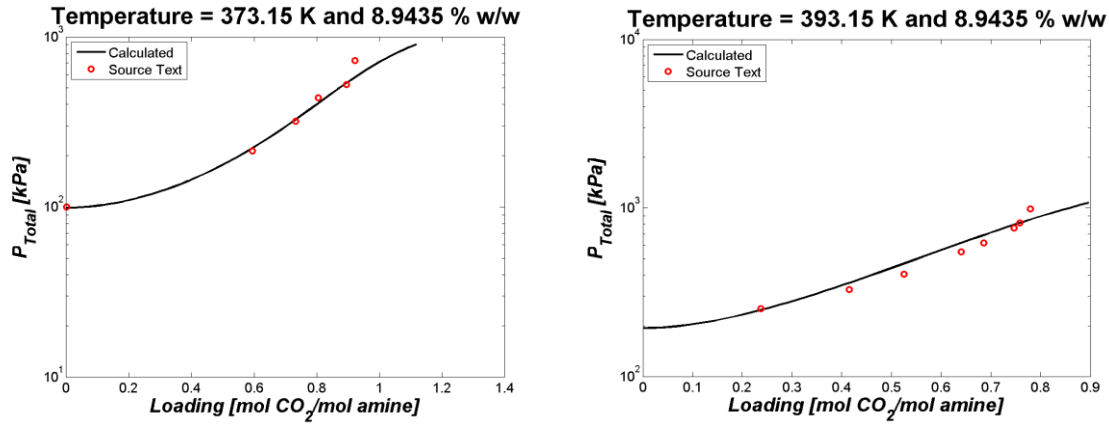

Figure 4.7 e-NRTL representation of CO_2 partial pressure over AMP-CO_2-H_2O system: experimental data: this work; solid lines e-NRTL mode

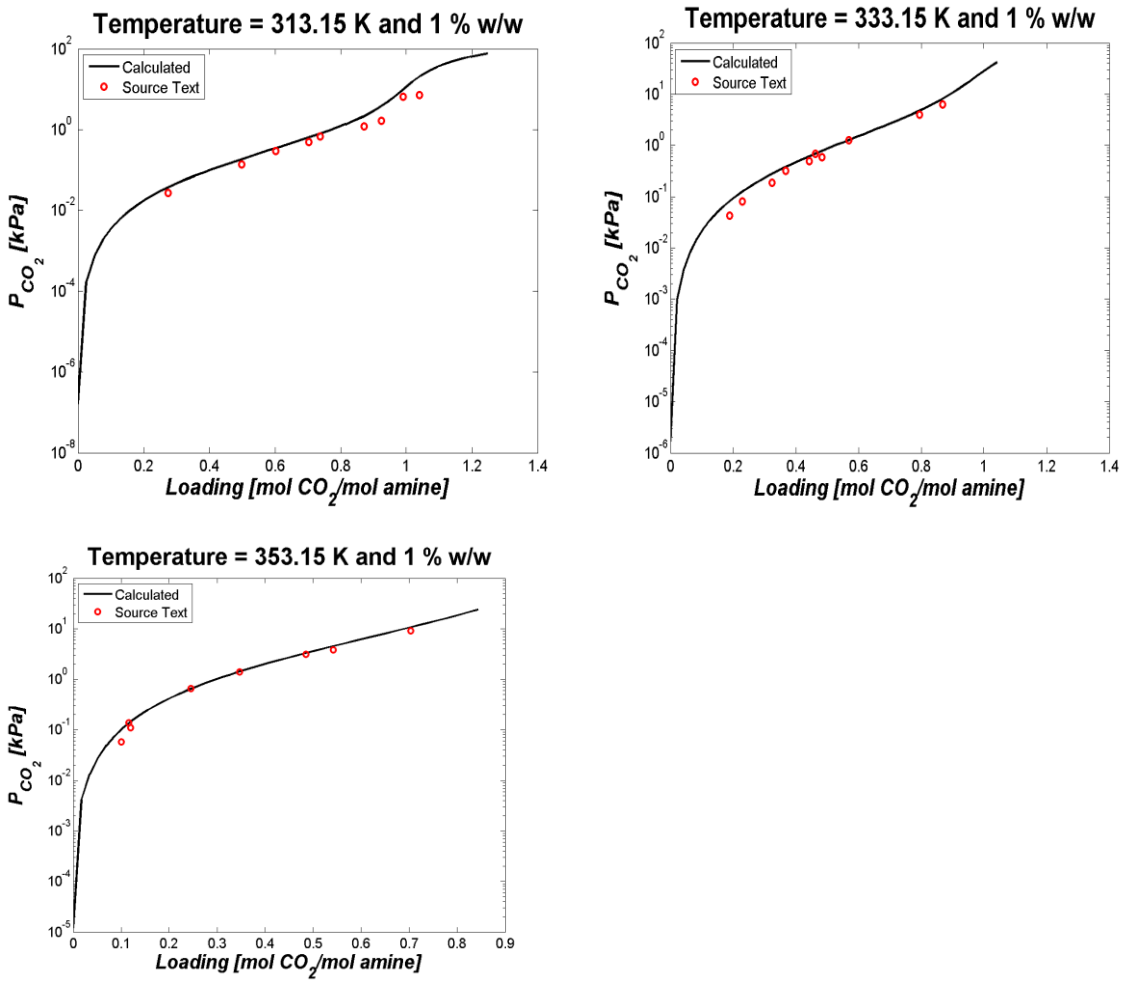

Figure 4.8 e-NRTL representation of CO_2 partial pressure over AMP-CO_2-H_2O system: experimental data: this work; solid lines e-NRTL mode

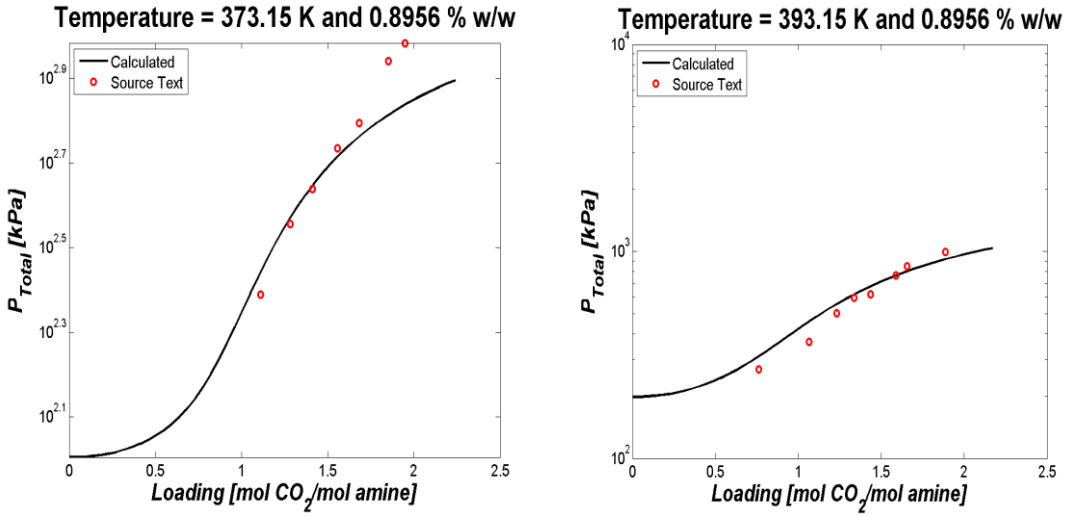

Figure 4.9 e-NRTL representation of total pressure over AMP-CO_2-H_2O system: experimental data: this work; solid lines e-NRTL mode

Accuracy of the Model

Figure (4.10) and (4.11) show the parity plot of experimental pressures(P_{CO2} and total pressure) and model prediction pressures results. From the figures it can be seen that the model results are in excellent agreement with the experimental results. Only the model does not predict few data points but overall it looks good. The AARD for P_{CO2} and P_{total} is 16.9% and 9.4% respectively, which is relatively an acceptable value.

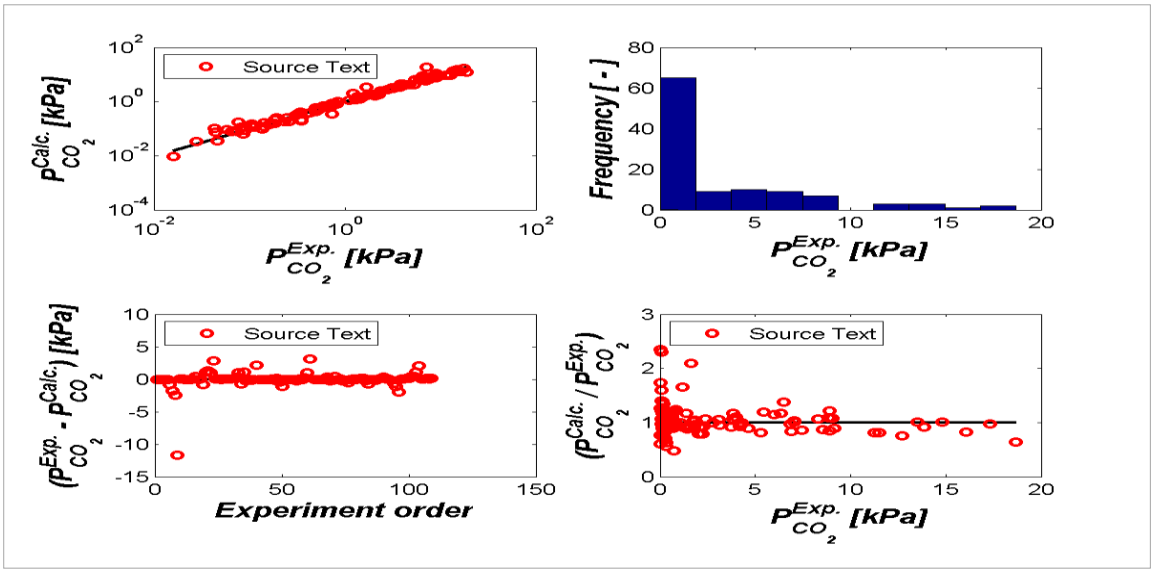

Fig 4.10 Parity plot between experimental and model predicted CO_2 partial pressure

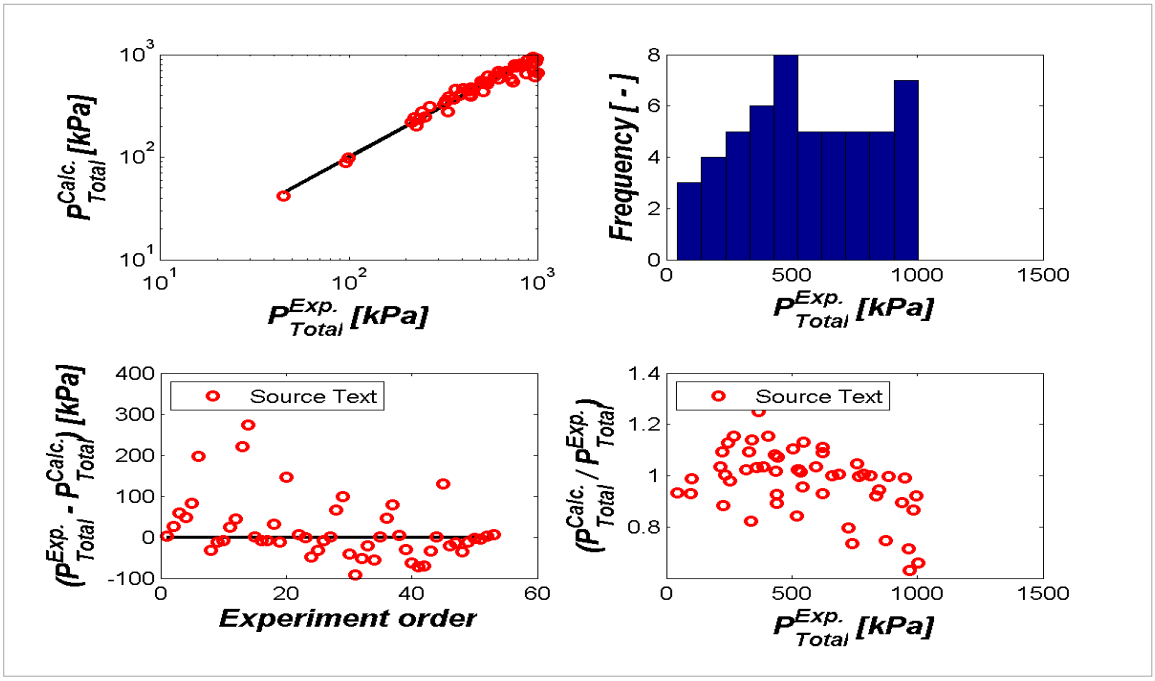

Fig 4.11 Parity plot between experimental and model predicted total pressure

4.2.3 Ternary System (Case2)

CO_2 can either be bounded chemically in an absorbent or remain free in the absorbent (physical solubility). Physical solubility of CO_2 in an absorbent at various concentrations and temperatures is necessary in the development of kinetics and thermodynamic model for the system. The problem is that CO_2 reacts with solvent. This reactive nature of CO_2 does not allow to measure the physical solubility of CO_2 in the solution. The N_2O analogy can be used to measure the physical solubility of CO_2 as explained in section 2.2.4. The use of N_2O solubility in the model calculation enables determination of CO_2 activity coefficient.

4.2.3.1 Ternary interaction parameters regression with physical solubility data

The discussion in case 1, the ternary parameters were regressed using the experimental CO_2 partial pressure and total pressure only. In case 2, the interactions parameters were regressed again using the experimental CO_2 partial pressure, total pressure and experimental physical solubility data. The regression analysis was performed through the optimization method PSO (lbest) using the MATLAB based parameter estimation tool, *Modfit* (Diego Di. D Pinto and Juliana Monteiro) The objective function used to minimize the error is given as:

$$AARD\% = \frac{1}{NP}\left[\sum\left(\frac{{P_{CO2}}^{exp} - {P_{CO2}}^{calc}}{{P_{CO2}}^{exp}}\right) + \sum\left(\frac{{P_{total}}^{exp} - {P_{total}}^{calc}}{{P_{total}}^{exp}}\right) + \sum\left(\frac{{H_{CO2}}^{exp} - {H_{CO2}}^{calc}}{{H_{CO2}}^{exp}}\right)\right].100$$

Regressed ternary interaction parameters for AMP-CO_2-H_2O system are given in the table 4.3

Table 4.3 Regressed ternary e-NRTL parameters without physical solubility data

Legend									
1	H_2O		4	H_3O^+		7	HCO_3^-		
2	CO_2		5	$AMPH^+$		8	CO_3^{-2}		
3	AMP		6	OH-		9	AMPCO2-		
	a (-)		**b (K)**	**Source**		**a (-)**		**b (K)**	**Sourse**
a1,4-6	8	**b1,4-6**	0	Default	**a4-6,1**	-4	**b4-6,1**	0	Default
a1,4-7	8	**b1,4-7**	0	Default	**a4-6,2**	-8	**b4-6,2**	0	Default
a1,4-8	8	**b1,4-8**	0	Default	**a4-6,3**	-6.01087	**b4-6,3**	-219.188	Regressed
a1,4-9	7.832533	**b1,4-9**	-1187.52	Regressed	**a4-7,1**	-11.7758	**b4-7,1**	407.8511	Default
a1,5-6	-3.76317	**b1,5-6**	-969.812	Regressed	**a4-7,2**	-4	**b4-7,2**	0	Default
a1,5-7	-17.2473	**b1,5-7**	-124.236	Regressed	**a4-7,3**	-8	**b4-7,3**	0	Regressed
a1,5-8	-23.009	**b1,5-8**	568.4811	Regressed	**a4-8,1**	-16.1944	**b4-8,1**	-849.011	Regressed
a1,5-9	-10.477	**b1,5-9**	-1120.74	Regressed	**a4-8,2**	-8.24287	**b4-8,2**	534.4281	Regressed
a2,4-6	15	**b2,4-6**	0	Default	**a4-8,3**	-4	**b4-8,3**	0	Regressed
a2,4-7	15	**b2,4-7**	0	Default	**a4-9,1**	-8	**b4-9,1**	0	Regressed
a2,4-8	15	**b2,4-8**	0	Default	**a4-9,2**	-13.0005	**b4-9,2**	-520.63	Regressed
a2,4-9	-0.9751	**b2,4-9**	1023.136	Regressed	**a4-9,3**	35.16708	**b4-9,3**	-728.198	Regressed
a2,5-6	10.5179	**b2,5-6**	-595.813	Regressed	**a5-6,1**	20.93519	**b5-6,1**	62.32067	Regressed
a2,5-7	18.84149	**b2,5-7**	-40.3112	Regressed	**a5-6,2**	2.377421	**b5-6,2**	-503.03	Regressed
a2,5-8	-31.0518	**b2,5-8**	-1375.23	Regressed	**a5-6,3**	23.48992	**b5-6,3**	-980.986	Regressed
a2,5-9	24.8363	**b2,5-9**	1.473167	Regressed	**a5-7,1**	0.798551	**b5-7,1**	-690.026	Regressed
a3,4-6	13.55051	**b3,4-6**	-1134.14	Regressed	**a5-7,2**	7.71965	**b5-7,2**	-737.334	Regressed
a3,4-7	-26.0763	**b3,4-7**	191.2908	Regressed	**a5-7,3**	-3.31926	**b5-7,3**	68.37399	Regressed
a3,4-8	-6.9229	**b3,4-8**	315.7257	Regressed	**a5-8,1**	-1.18221	**b5-8,1**	-171.466	Regressed
a3,4-9	25.84428	**b3,4-9**	-1010.07	Regressed	**a5-8,2**	-15.2405	**b5-8,2**	-1283.23	Regressed
a3,5-6	-21.6349	**b3,5-6**	-764.274	Regressed	**a5-8,3**	9.348766	**b5-8,3**	-1668.44	Regressed
a3,5-7	-17.3206	**b3,5-7**	-606.579	Regressed	**a5-9,1**	3.384707	**b5-9,1**	-432.068	Regressed
a3,5-8	-16.01	**b3,5-8**	-449.973	Regressed	**a5-9,2**	-20.2913	**b5-9,2**	-492.058	Regressed
a3,5-9	-10.7209	**b3,5-9**	-918.686	Regressed	**a5-9,3**	-2.87738	**b5-9,3**	-348.569	Regressed

4.2.3.2 Full model prediction AMP-CO_2-H_2O

The estimated interaction parameters for AMP-CO_2-H_2O system presented in table 4.1 and 4.3 are used to predict VLE of aqueous AMP using e-NRTL model. The model prediction results along with the experimental results are shown in the Figure 4.13 (a-f).

It can be seen that the model predictions of CO_2 partial pressure and total pressure are in good agreement with experimental data over all temperature ranges. But the AARD for CO_2 partial pressure and total pressure are 20.7% and 14.26% respectively. These deviations have higher value than reported in case 1. The reason of high deviations is that the interaction parameters determined using the experimental VLE (CO_2 partial pressure and tptal pressure) data along with physical solubility data. The model prediction results for N_2O solubility are shown in figure (4.12) with in an AARD of 31.75%. The AARD value of 31.75% indicates that the model representation is not in good agreement with the experimental solubility data. The reason of this disagreement may be the error in the model calculations. In the parameters estimations a large quantity of experimental data points (more then 150) are used. It is common that using large quantity of data sets increase the deviation between the experiments and model predictions. The error in the experimental data is also the reason of variations in the experimental and model results. The figure (4.12) shows that some experimental data points are completely off and scattered. This is also the reason of high deviation in model and experimental results.

It can be observed from the figure 4.13(c) there is a convergence problem at 40^0C over 1M (9wt%) AMP. This may be due to the model calculations for the chemical equilibria at this specific loading.

The model prediction results and experimental CO_2 partial pressure and total pressure for all AMP concentrations are shown in figure 4.13(a-f). Overall the model is seen to predicts well the CO_2 partial pressure but it over predict the values of total pressure for 1M(8.9% w/w) and 0.1M(0.89%w/w).

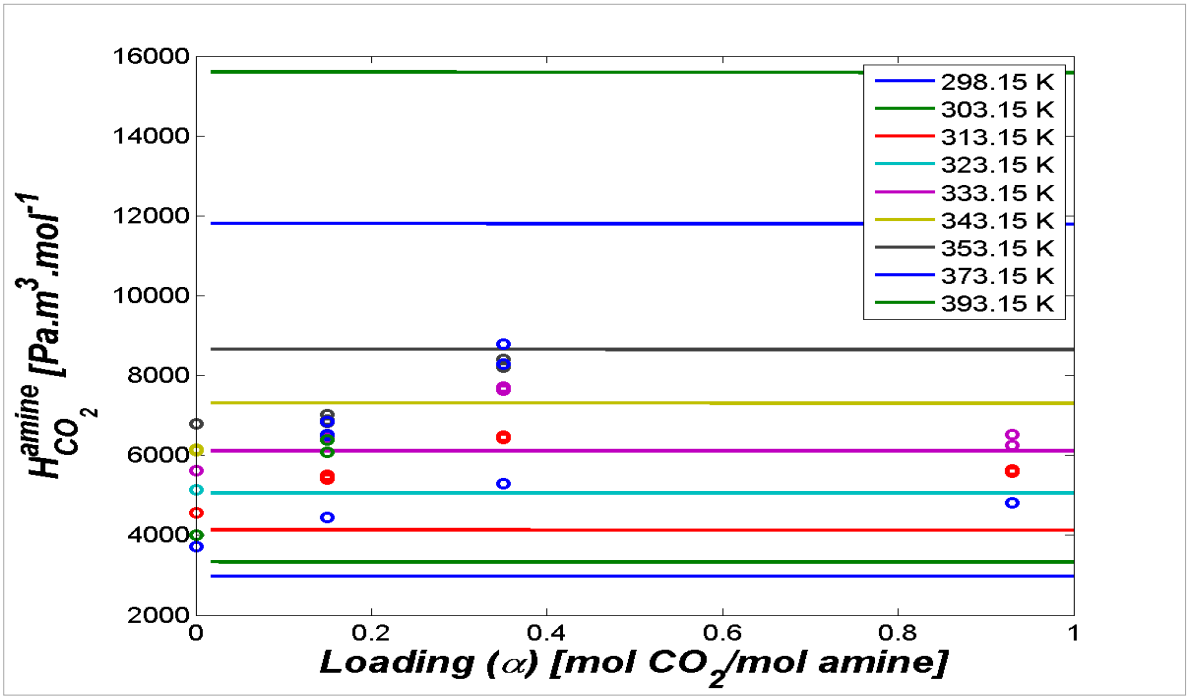

Figure 4.12 Henry's law constant of CO_2 in 26.84% AMP at various loading: experimental point this work; lines e-NRTL model

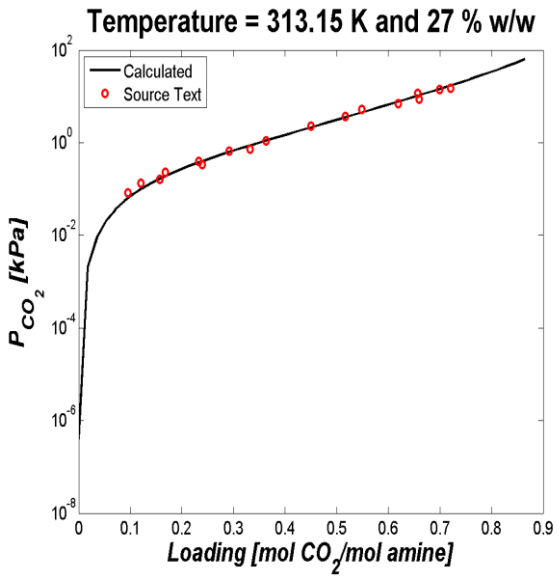

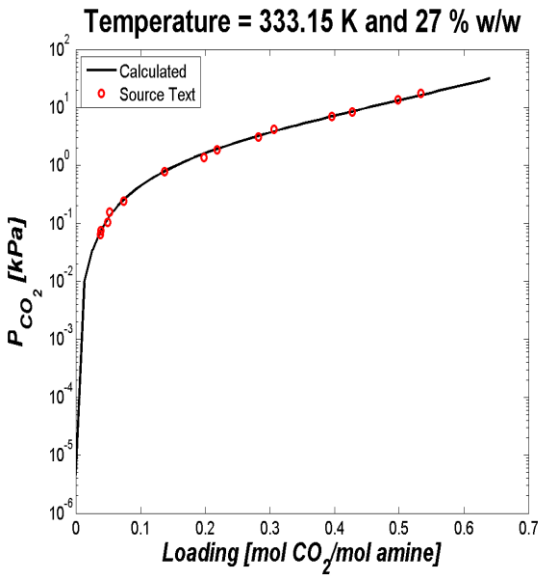

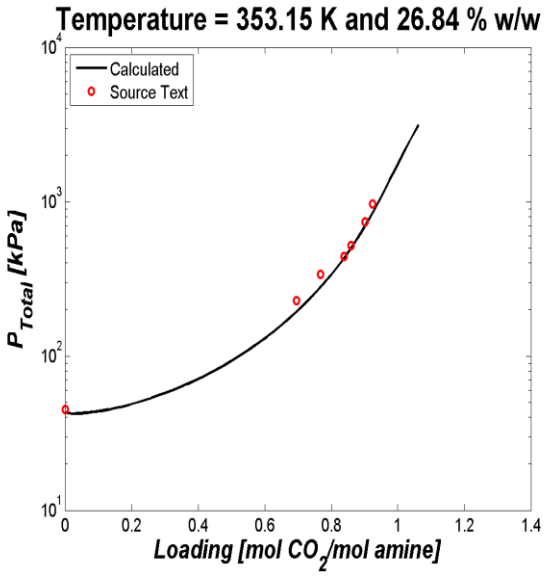

Figure 4.13: (a) Model representation of CO_2 partial pressure over AMP-CO_2-H_2O system: experimental data: this work; solid lines, e-NRTL model

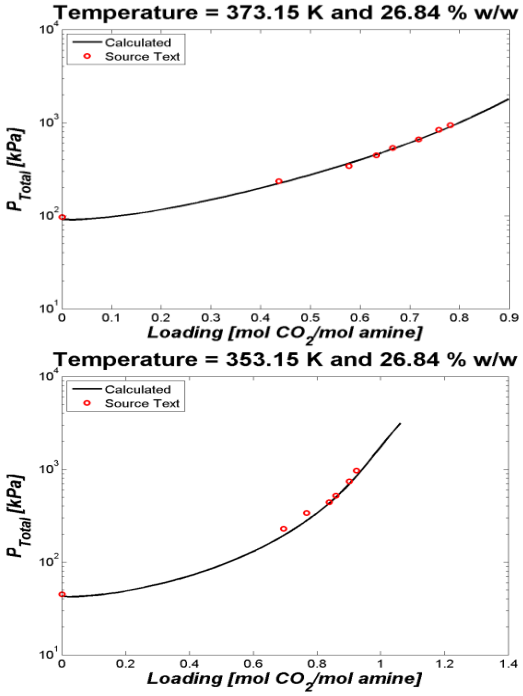

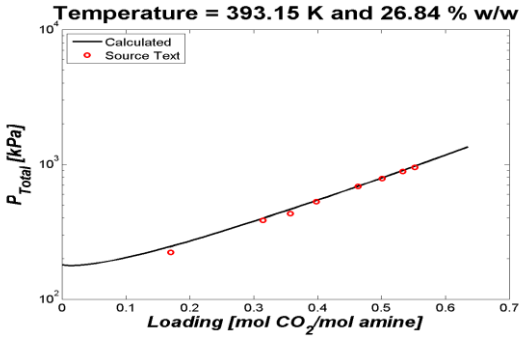

Figure 4.13: (b) Model representation of total pressure over AMP-CO_2-H_2O system: experimental data: this work; solid lines e-NRTL model

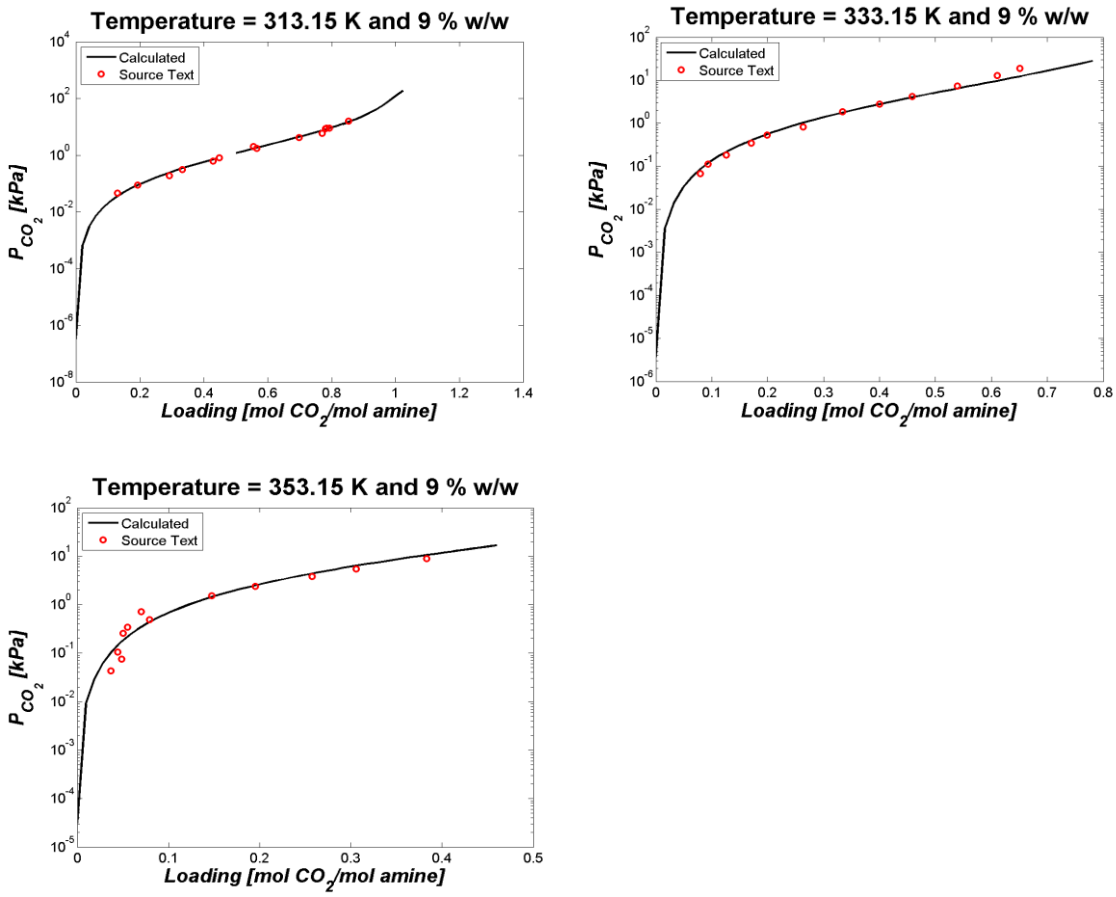

Figure 4.13 (c) Model representation of CO_2 partial pressure over AMP-CO_2-H_2O system: experimental data: this work; solid lines, e-NRTL model

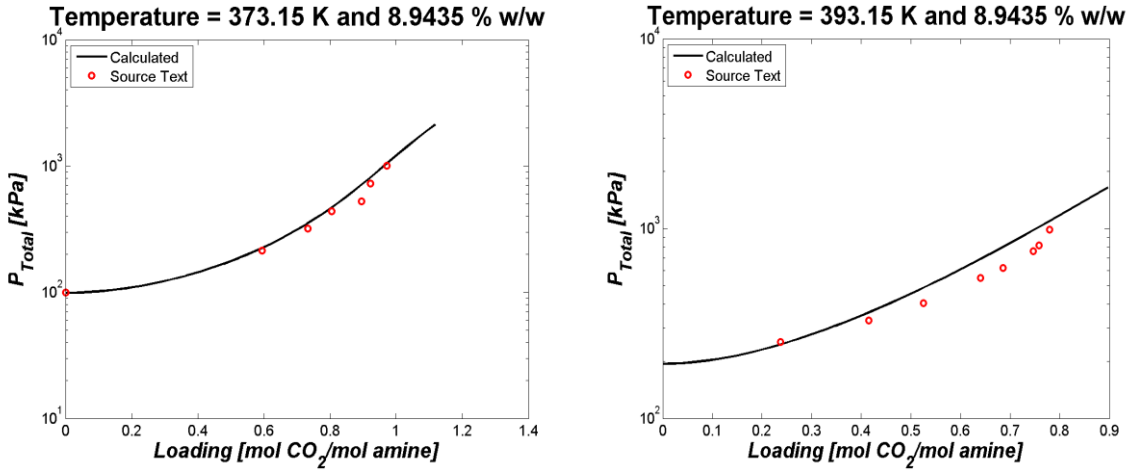

Figure 4.13 (d) Model representation of total pressure over AMP-CO_2-H_2O system: experimental data: this work; solid lines e-NRTL model

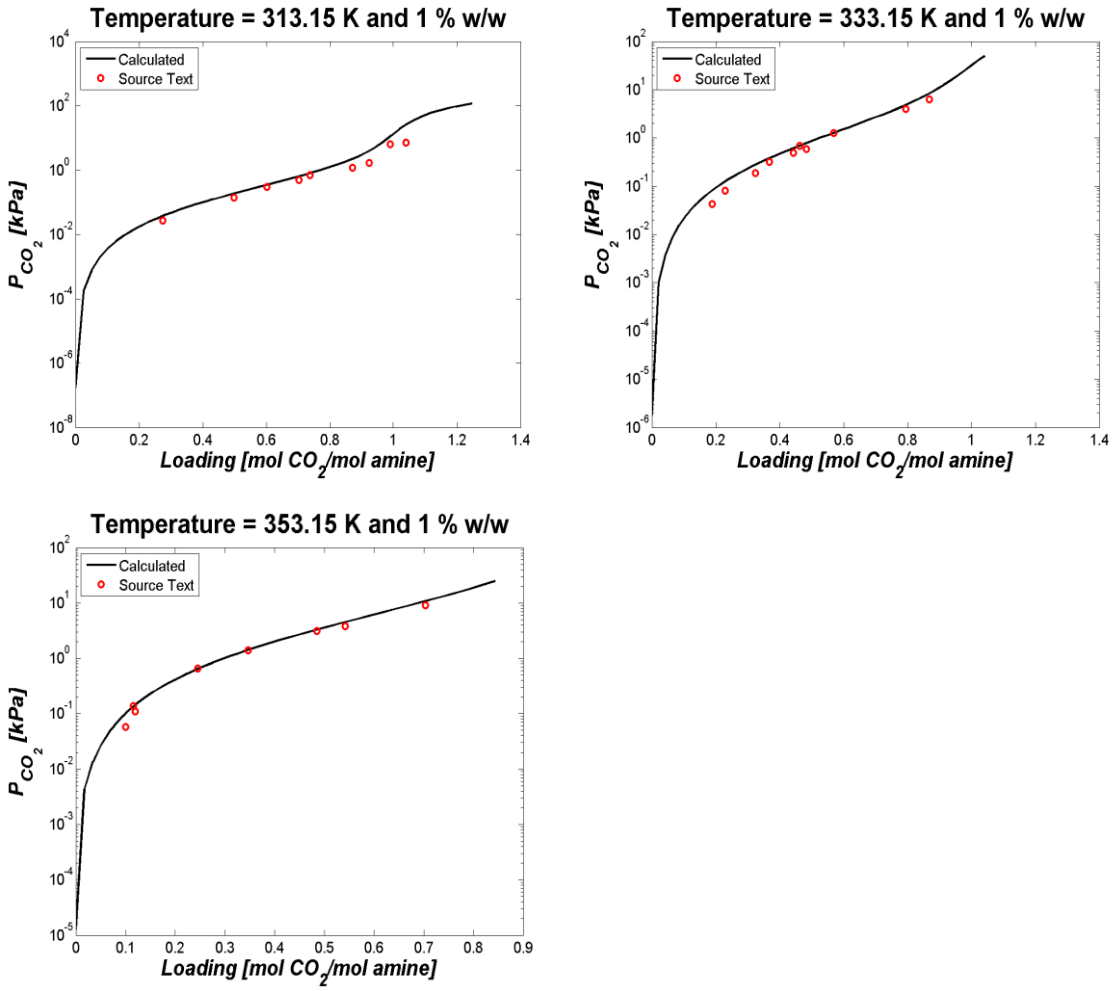

Figure 4.13 (e) Model representation of CO_2 partial pressure over AMP-CO_2-H_2O system: experimental data: this work; solid lines, e-NRTL model

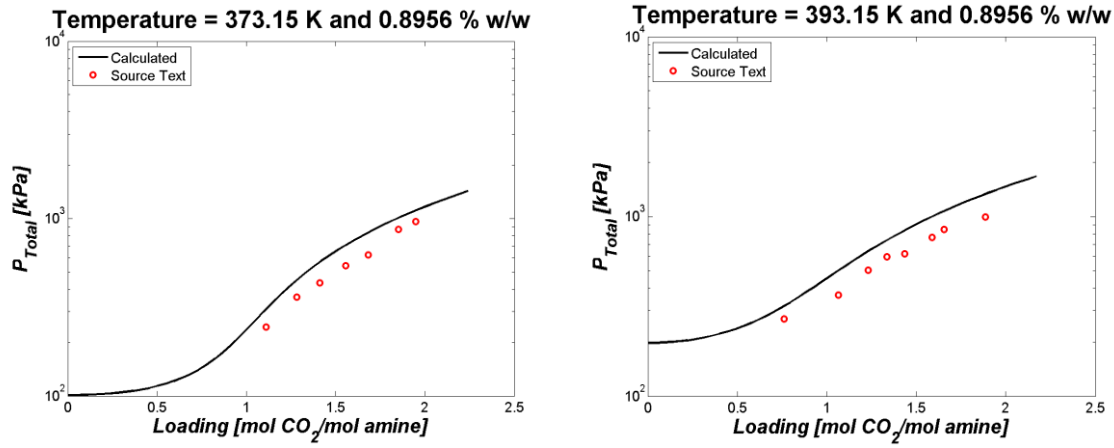

Figure 4.13 (f) Model representation of total pressure over AMP-CO_2-H_2O system: experimental data: this work; solid lines, e-NRTL model

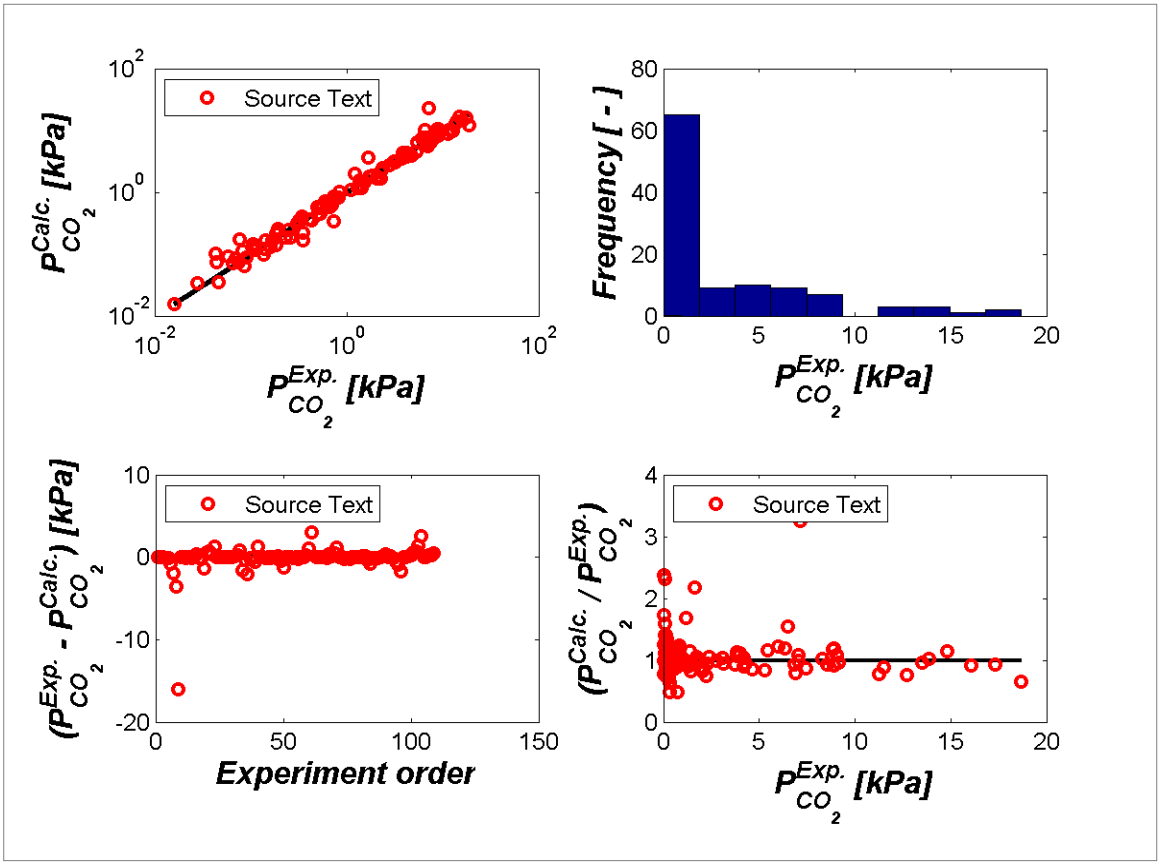

Figure 4.14 (a) Parity plot between experimental and model predicted CO_2 partial pressure:

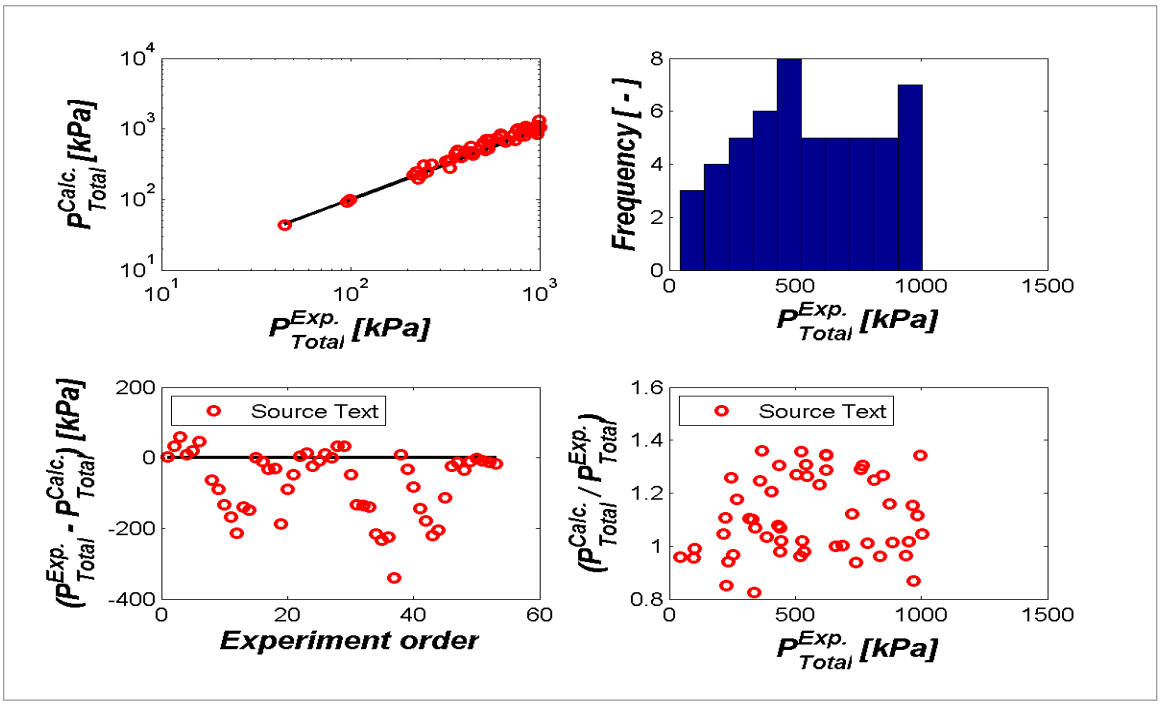

Figure 4.14(b) Parity plot between experimental and model predicted total pressure:

4.2.4 Speciation

An important observation from rigorous thermodynamic modeling of VLE of CO_2 in aqueous AMP is the determination of the concentration profile. The model predicted activity coefficients of each species in liquid phase are used to determine the liquid phase equilibrium concentrations of various species as a function of loading (mole of CO_2/ mole of amine) as shown in the figure 4.15. It is clear from the figure that AMP disappear with the CO_2 loading and carbamate formation is very low. The protonated AMP and bicarbonate are the main reaction product.

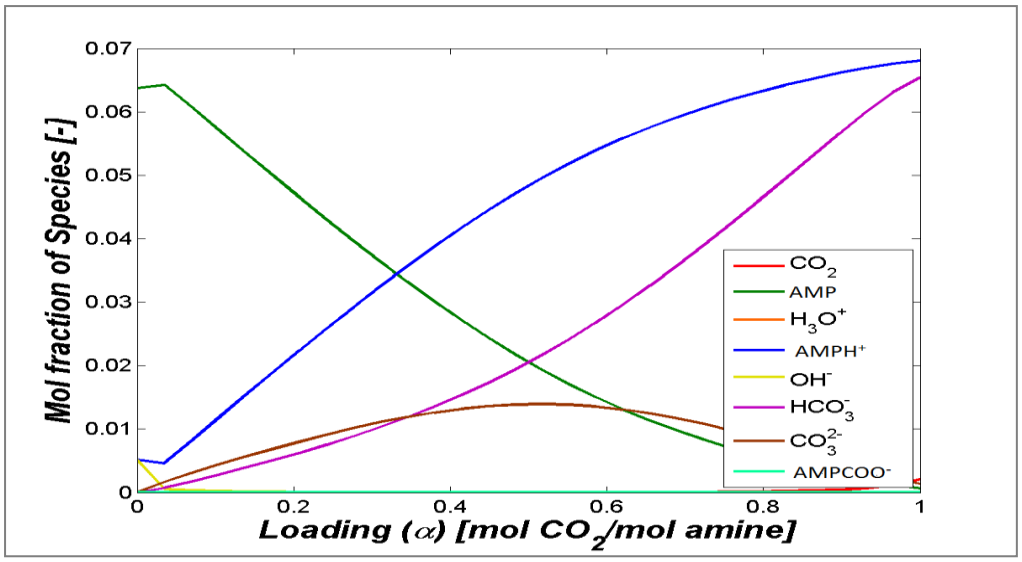

Figure 4.15 Liquid phase speciation

Conclusions

New experimental data for vapor-liquid equilibrium of CO_2 in aqueous solutions of 3M/26.84% wt, 1M/9% wt and 0.1M/0.89% wt AMP (2-amino-2-methyl-1-propanol) and 1.5M PZ are reported from 313 to 393K. Low pressure/temperature equilibrium apparatus was used to measure the CO_2 partial pressure over loaded AMP solutions while total pressure was measured with high pressure/temperature equilibrium apparatus. The experiments cover the temperature range of (313K–353K) and CO_2 partial pressure range of (0.0207-18.67KPa) for AMP solutions. The experiments also present total pressure range (222.4-1001.9KPa) and (222.4-973.9KPa) for AMP and PZ systems at temperature range of (353-393K) respectively. A thermodynamic model representing the AMP system was developed using the e-NRTL framework. The binary interaction parameters (molecule-molecule) for AMP-H_2O system were regressed using binary VLE data and excess enthalpy data from literature in NRTL equation. Then these binary interaction parameters were fixed and regressed the ternary interaction parameters using the VLE data and physical CO_2 solubility data of this work. The model gives a good representation of experimental binary VLE data and excess enthalpy data with an AARD of 0.01% and 5.9% respectively. The model also gives an excellent agreement for CO_2 partial pressure and total pressure for all AMP concentrations with an AARD of 20.7% and 14.26 % while the physical solubility data was predicted with in an AARD of 31.7579%. Further, the model predicts the liquid phase speciation.

Recommendations

The experimental data on apparent Henry's law constant that encompasses the CO_2 activity coefficient at different loading (using the N_2O analogy) was used for parameters fitting in the e-NRTL model. The model shows larger deviations from experimental data. Model needs to be improved in future for the better fitting of the experimental data.

Model needs to be improved in terms of beter parameter fitting based on experimental data of freezing point depression and heat of absorption.

For low pressure VLE measurements, manual CO_2 loading was done. It is recommended that loaded solution should not be used for further loading, it may cause the amine loss (resulting in changed concentration). Fresh solution should be loaded only once.

References

Astarita G., Savage D.W., and Bisio A. (1983) Gas treating with chemical solvents. John Wiley and Sons.

Born, M. Volumen und Hydrationswärme der Ionen, Z. Phys. 282 (2) (1920)

C. Chen, C. Bokis and P. Mathias. Segment-based excess gibbs energy models for aqueous organic electrolytes, A.I.Ch.E. J. 47 (11) (2001)

C-C. Chen and Song,Y, 2004. Generalized electrolyte NRTL model for mixed solvent electrolyte systems,A.I.Ch.E. J. 50 (8) (2004)

Chen, C.-C. and Evans, L.B. A Local Composition Model for the Excess Gibbs Energy of Aqueous Electrolyte systems, AIChE J., 32, (1986)

Clarke, J. K. A., 1964, Kinetics of Absorption of Carbon Dioxide in Monoethanolamine Solutions at Shorts Contact Time, Ind. Eng. Chem. Fundam., 3, 239-245

Denbigh, K.G. (1984). The principle of chemical equilibrium . 4th ed. Cambridge University press, pp.494

Diego, D.D., Monteiro, J., Regression model, 2012. Norwegian University of Science and Technology, CO_2 research group (PhD students)

Edwards, T.J., Maurer, G., Newman, J., Praunstiz,J. M., 1978. Vapor liquid equilibria in multicomponent aqueous solutions of volatile weak electrolytes. AlChE Journal, 24, 966-976.

Elliot,J.R; Lira, C.T.,1999. Introductory chemical engineering thermodynamics; Prentice hall PTR: New Jersey.

Environmental Protection Agency 2002, Inventory of U.S. Greenhouse Gas Emissions and Sinks: 1990-2000. Washington DC: Office of Atmospheric Programs

Folger, Peter, Carbon Capture: A Technology Assessment, Specialist in Energy and Natural Resources Policy July 19, 2010

Gabrielsen, J., Svendsen, F. Hallvard, Michelsen, L.M., Stenby, H. E.,Kontogeorgis, M. G.,Georgios M. Kontogeorgis, 2007, Experimental validation of a rate-based model for CO2 capture using an AMP solution, Chemical Engineering Science 62 ,pp 2397 – 2413

Gabrielsen, Jostein, Michelsen, M.L., Stenby H. Erling, Kontogeorgis, M. G., 2006, Modeling of CO_2 Absorber Using an AMP Solution , Wiley Inter Science

Gupta, Mayuri. Computational study of pKa and carbamate stability constant values for amines important in post combustion CO_2 capture prosess. NKS Annual meeting in Computational Chemistry, 2012(in progress)

Harned, H.S. and Owen, B.B. The Physical Chemistry of Electrolytic Solutions (third ed.), New York, Reinhold Publishing Corp (1958)

Hartono et al., 2012 (in progress)

IEA Energy Technology Essentials. CO_2 Capture & Storage. (2004a)

Kim ,I., Hoff, A. K., Hessena, T.E., Haug-Warberga, T., Svendsen, F. H. Enthalpy of absorption of CO_2 with alkanolamine solutions predicted from reaction equilibrium constants. Chemical Engineering Science 64 (2009) 2027 -- 2038

Kim, I., Jens, M. C., Grimstvedt, A., Svendsen, F. H. Thermodynamics of protonation of amines in aqueous solutions at elevated temperatures.J. Chem. Thermodynamics 43 (2011) 1754–1762.

Kim,Inna. Heat of reaction and VLE of post combustion CO_2 absorbants. Doctoral theses at NTNU, 2009

Kohl, L. A., Nielsen, B.R.,1997, Gas Purification, Gulf Professional Publishing

Kundu, M., Mandal, P. B. and Bandyopadhyay, S.S. 2003. Solubility of CO_2 in 2-Amino-2-methyl-1-propanol Solutions. J. Chem. Eng. Data , 48, 789-796

Laddha, S. S., Diaz, J. M., Danckwerts, P. V., 1981, the N2O Analogy: the Solubilities of CO_2 and N_2O in Aqueous Solutions of Organic Compounds, Chem. Eng. Sci., 36, 228-229.

Ma'mun, S., Jakobsen, P. J., Svendsen, F. H., Jana P., Juliussen, O. Experimental and Modeling Study of the Solubility of Carbon Dioxide in Aqueous 30 Mass % 2-((2-Aminoethyl) amino) ethanol Solution. Ind. Eng. Chem. Res. 2006, 45, 2505-2512

Ma'mun, S., Nilsen , R., Svendsen, F. H., Juliussen, O. Solubility of Carbon Dioxide in 30 mass % Monoethanolamine and 50 mass% Methyldiethanolamine Solutions. *J. Chem. Eng. Data* 2005**,** *50,* 630-634

Mandal B.P., Kundu M. and Bandyopadhyay S.S.," Physical solubility and diffusivity of N2O and CO2 into aqueous solutions of (2-amino-2-methyl-1-propanol+monoethanolamine) and (N-methyldiethanolamine+monoethanolamine)", J. Chem. Eng. Data, 50 2 (2005), pp. 352–358.

Mathonat, C., Maham, Y.,Hepler, G.1997. Excess Molar Enthalpies of (Water + Monoalkanolamine) Mixtures

Pitzer, K. S. Electrolytes from dilute solution to fused salts. Journal of the American Chemical Society, 102(9), (1980)

Prausnitz, J. M., Lichtenthaler, R. N., Gomes, de Azevedo E., " Molecular Thermodynamics of Fluid-Phase Equilibria", 3rd ed. Prentice Hall PTR: Upper Saddle River, N.J., 1999

Renon,H.,J.M. Prausnitz,"Estimation of parameters for the NRTL equation for Excess Gibbs energies of strongly non-ideal liquid mixtures, 1969

Roberts, B. E., and Mather, A.E., Chem. Eng. Commun.64 (1988)

Sartori, G., Savage, W. D., 1983, Sterically hindered amines for carbon dioxide removal from gases, Ind. Eng. Chem. Fundamen., 22 (2), pp 239–249

Sharma, M. M.,1965, Kinetics of reactions of carbonyl sulphide and carbon dioxide with amines and catalysis by Brönsted bases of the hydrolysis of COS.

Soren Anderson and Richard Newell, 2003, Prospects for Carbon Capture and Storage Technologies, Washington DC, 20036

Sukanta Kumar Dash et al, 2011, (Vapour + liquid) equilibria (VLE) of CO_2 in aqueous solutions of 2-amino-2-methyl-1-propanol: New data and modelling using eNRTL-equation

Thomsen, K., 2006. Thermodynamics of Electrolyte Solutions, Department of Chemical Engineering, DTU, 2006

Tontlwachwuthlkul, P., Melsen, A. Llm, J.C. 1991. Solubility of CO_2 in 2-Amino-2-methyl-1-propanol Solutions. J. Chem. Eng. Data IQQ1, 36, 130-133

Yang Z.Y.,Soriano A.N.,Caparanga A.R.,Li, M.H. Equilibrium solubility of carbon dioxide in (2-amino-2-methyl-1-propanolþpiperazine+water). J. Chem. Thermodyn. 42, 659–665,(2010)

Zhang, K., Hawrylak, B., Palepu, R., Tremaine, R.P.2002. Thermodynamics of aqueous amines: excess molar heat capacities, volumes, and expansibilities of {water + methyldiethanolamine (MDEA)} and {water +2-amino-2-methyl-1-propanol (AMP)}

List of appendices

Appendix
Appendix A: VLE Data for amine systems (this work)

Table A1 Experimental equilibrium data points of P_{CO2}, P_{total} and Loading for system 3M (26.88% w/w) AMP at 40, 60, 80, 100 and 120 ^{0}C

(Red points are reproduced data)

40°C		60 °C		80 °C		80 °C		100 °C		120 °C	
Loading	PCO_2	Loading	PCO2	Loading	PCO2	Loading	Ptotal	Loading	Ptotal	Loading	Ptotal
nCO2/nAm	KPa	nCO2/nAm	KPa	nCO2/nAm	KPa	nCO2/nAm	KPa	nCO_2/nAm	KPa	nCO_2/nAm	KPa
0.0956	0.0837	0.0379	0.0636	0.0052	0.0156	0.0001	44.9	0.0001	96.3	0.1705	222.40
0.1206	0.1331	0.0491	0.1052	0.0229	0.1825	0.6961	227.9	0.4362	235.10	0.3149	385.20
0.1572	0.1635	0.0738	0.2421	0.0252	0.3431	0.7673	337.1	0.5775	340.90	0.3577	431.60
0.1678	0.2308	0.1375	0.7836	0.0734	1.4127	0.8388	441.4	0.6328	445.40	0.3978	528.90
0.2326	0.3943	0.2183	1.8424	0.0897	2.2487	0.8592	519.4	0.6657	533.60	0.4636	686.10
0.2915	0.6631	0.3061	4.2073	0.1456	4.6591	0.9016	741.5	0.7177	659.60	0.5012	785.10
0.3631	1.0987	0.3960	7.0430	0.1739	6.8967	0.9236	968.3	0.7585	836.30	0.5331	886.40
0.4501	2.2558	0.4982	13.5218	0.2221	11.2465			0.7816	938.10	0.5523	951.20
0.5165	3.7274	0.5334	17.3346	0.0379	0.4215						
0.5487	5.3098	0.0384	0.0740	0.0433	0.5233						
0.0000	0.0000	0.0524	0.1569	0.0929	2.0605						
0.6991	13.8543	0.1984	1.3597	0.1478	4.3031						
0.7205	14.8081	0.2825	3.1014	0.1874	6.8229						
0.2388	0.3406	0.4273	8.2910								
0.3323	0.7202										
0.6191	7.0393										
0.6568	11.5187										

Table A2 Experimental equilibrium data points of P_{CO2}, P_{total} and Loading for system 0.1M (0.89% w/w) AMP at 40, 60, 80, 100 and 120 °C

40 °C		**60 °C**		**80 °C**		**100 °C**		**120 °C**	
Loading	PCO2	Loading	PCO2	Loading	PCO2	Loading	Ptotal	Loading	Ptotal
nCO2/nAm	KPa	nCO2/nAm	KPa	nCO2/nAm	KPa	nCO2/nAm	KPa	nCO2/nAm	KPa
0.2748	0.0270	0.1889	0.0429	0.0998	0.0573	1.1105	245.20	0.7615	269.80
0.4982	0.1399	0.2291	0.0812	0.1157	0.1383	1.2809	359.90	1.0638	366.50
0.6020	0.2980	0.3241	0.1881	0.1196	0.1100	1.4104	434.60	1.2310	503.80
0.7036	0.4942	0.3682	0.3185	0.2451	0.6603	1.5571	542.80	1.3349	597.70
0.7383	0.6836	0.4430	0.4970	0.3465	1.3869	1.6818	622.20	1.4344	621.60
0.8711	1.1911	0.4619	0.6911	0.4846	3.1545	1.8526	872.00	1.5889	765.50
0.9247	1.6533	0.4832	0.5899	0.5422	3.8521	1.9485	963.20	1.6548	846.00
0.9903	6.4962	0.5695	1.2814	0.7032	9.0375			1.8877	994.90
1.0395	7.1374	0.7955	3.9657						
		0.8679	6.3194						

Table A3 Experimental equilibrium data points of PCO_2, P_{total} and Loading for system 1M (8.9% w/w) AMP at 40, 60, 80, 100 and 120^{0}C

40 °C		60 °C		80 °C		100 °C		120 °C	
Loading	**PCO2**	**Loading**	**PCO2**	**Loading**	**PCO2**	**Loading**	**Ptotal**	**Loading**	**Ptotal**
nCO2/nAm	**Kpa**	**nCO2/nAm**	**Kpa**	**nCO2/nAm**	**Kpa**	**nCO2/nAm**	**Kpa**	**nCO2/nAm**	**Kpa**
0.1302	0.0458	0.0798	0.0680	0.0367	0.0427	0.000001	99.9	0.2373	253.10
0.1933	0.0890	0.0932	0.1111	0.0445	0.1043	0.5944	213.80	0.4147	328.40
0.2927	0.1881	0.1261	0.1816	0.0487	0.0750	0.7332	318.40	0.5254	404.90
0.3331	0.3155	0.1705	0.3412	0.0501	0.2576	0.8057	438.70	0.6408	547.90
0.4288	0.6232	0.1992	0.5304	0.0551	0.3451	0.8958	523.40	0.6857	620.90
0.4492	0.8110	0.2635	0.8266	0.0702	0.7198	0.9230	725.40	0.7470	760.20
0.5555	2.0491	0.3338	1.8332	0.0790	0.4937	0.9727	1001.90	0.7581	814.20
0.5664	1.7161	0.4002	2.7723	0.1476	1.5235			0.7801	984.70
0.6991	4.2025	0.4584	4.2144	0.1954	2.3753				
0.7705	6.0132	0.5393	7.4230	0.2577	3.8517				
0.7809	8.5399	0.6103	12.7169	0.3061	5.4274				
0.7839	8.8946	0.6508	18.6703	0.3833	8.8744				
0.7934	9.1349								
0.8533	16.0470								

Table A4 Experimental equilibrium data points of PCO_2, P_{total} and Loading for system (1M AMP) at 40, 60, 80, 100 and 120 °C

40 °C		60 °C		80 °C		100 °C		120 °C	
Loading	PCO2	Loading	PCO2	Loading	PCO2	Loading	Ptotal	Loading	Ptotal
nCO2/nAm	Kpa	nCO2/nAm	Kpa	nCO2/nAm	Kpa	nCO2/nAm	Kpa	nCO2/nAm	Kpa
0.3690	0.0393	0.2349	0.0578	0.1018	0.0492	1.0152	830	0.6945	270.60
0.4811	0.1075	0.2746	0.0910	0.1498	0.1054	0.9996	535.6	0.7559	336.20
0.5098	0.1508	0.2961	0.1089	0.1640	0.1249	1.0195466	997.3	0.7903	423.30
0.5801	0.2808	0.4301	0.3437	0.1874	0.2034	1.020611	860.6	0.8659	551.60
0.6567	0.7711	0.4653	0.5086	0.2607	0.3973	1.013279	742.7	0.8703	636.60
0.7017	1.2926	0.5396	0.9324	0.3600	0.8268	0.9430329	345.7	0.9232	789.30
0.7651	3.5309	0.6098	2.0897	0.4325	1.8190	0.8708348	253.6	0.9564	877.70
0.7913	4.3927	0.6951	5.4983	0.5287	4.0163				
		0.7637	10.2421	0.6082	8.7926				
		0.7848	15.4043	0.6376	10.7112				

Table A5 Solubility data of 3(26.84% w/w)AMP Loaded

Temperature	Loading	Weight fraction	Henry's Constant
°C	nCO2/nAm	(-)	kPa m3 mol-1
120	0.15	0.2688	10.48247961
120	0.15	0.2688	9.994154466
100.04	0.15	0.2688	10.90181806
100.04	0.15	0.2688	10.33079758
100	0.15	0.2688	10.38068479
80	0.15	0.2688	10.56377664
80	0.15	0.2688	10.46210027
80	0.15	0.2688	10.76111841
60	0.15	0.2688	9.544819659
60	0.15	0.2688	9.520531219
60	0.15	0.2688	9.424004088
40	0.15	0.2688	7.738524845
40	0.15	0.2688	7.701428216
40	0.15	0.2688	7.6111445
25	0.15	0.2688	6.026771625
100	0.35	0.2688	13.96384789

Temperature	Loading	Weight fraction	Henry's Constant
°C	nCO2/nAm	(-)	kPa m3 mol-1
60	0.35	0.2688	11.36462836
40	0.35	0.2688	9.103798594
25	0.35	0.2688	7.151669912
40	0.35	0.2688	9.048245647
60	0.35	0.2688	11.2311153
80	0.35	0.2688	12.60329652
100	0.35	0.2688	13.18579367
60	0.93	0.2688	9.589270228
40	0.93	0.2688	7.930426602
25	0.93	0.2688	6.506543632
40	0.93	0.2688	7.85571231
60	0.93	0.2688	9.217606153

Appendix B: Literature VLE Data

Table B1: Experimental equilibrium data points of PCO_2 and Loading for system (3M AMP) at 40, 60, 80°C

Roberts & mather 1988		Yang et al., 2010		Tontlwachwuthlkul et al.,1991					
40 °C		40 °C		40 °C		60 °C		80 °C	
loading	PCO2	loading	PCO2	Loading	PCO2	Loading	PCO2	Loading	PCO2
nCO2/nAm	Kpa	nCO2/nAm	Kpa	nCO2/nAm	Kpa	nCO2/nAm	Kpa	nCO2/nAm	Kpa
0.404	1.25	0.385	0.89	0.875	94	0.809	82.66	0.524	53.33
0.564	2.79	0.473	1.9	0.815	47.05	0.683	41.14	0.394	25.84
0.604	3.54	0.547	2.96	0.714	18.01	0.546	16.46	0.247	10.4
0.728	12.8	0.606	4.83	0.643	7.94	0.427	8	0.169	4.99
0.769	19	0.726	14.18	0.582	2.7	0.321	1.9	0.126	1.59
0.786	15.6	0.817	36.96						
0.818	22.5	0.885	82.65						
0.835	36.6	0.939	151.9						
0.919	99.5								
0.948	144								

Appendix C: VLE Calculations

Table C1: Calculations of Partial Pressure of CO_2 from atmospheric pressure and observed temperatures (60 0C) by subtraction of partial pressures of water and amine at given temperatures (3M AMP)

No	T_{bath}	T_{cooler}	T_{cell}	x_{H2O}	x_{Amine}	Psol @ Tcell	Psol @ Tcooler	P ambient		CO2 analyser	%CO2 analyser	%CO2 real	PCO2	Loading
	°C	°C	°C			(kPa)	(kPa)	(mmHg)	(kPa)	(Amp)	(%)	(%)	(kPa)	
VLE-1	60.8	14.3	60	0.9310	0.0690	17.3406	0.5045	771.8	102.898	10.8300	2.1700	2.15108	1.8513	0.22
VLE-2	60.8	14.4	60.1	0.9310	0.0690	17.4225	0.5045	771.8	102.898	20.3400	5.1600	4.91671	4.2274	0.31
VLE-3	60.7	14.6	60.1	0.9310	0.0690	17.4225	0.5045	771.8	102.898	9.8600	7.4000	8.22869	7.0750	0.4
VLE-4	60.6	14.9	60	0.9310	0.0690	17.3406	0.5045	771.8	102.898	19.6800	19.8000	20.22489	17.4059	0.53
VLE-5	60.6	14.8	60	0.9310	0.0690	17.3406	0.5045	771.8	102.898	16.0400	15.2000	15.77823	13.5790	0.5

W_{AMP}	**534.84**
W_{Pz}	0
W_{H2O}	1458.4
M_{AMP}	89.14
M_{Pz}	0
M_{H2O}	18.02
$\rho_{fresh\ sol}$	0.9966
C_{Amine}	3.010
	3.000

Table C2 Calculations of loading molCO2/mol amine from CO_2 analysis and amine analysis data (3M AMP)

		Remarks		Sample			Blank				Total CO2	[Amine]		loading	loading*
No	**Name**	**a**	**t/C**	**weight (g)**	**HCL(g)**	**NaoH(ml)**	**HCL(g)**	**NaoH(ml)**	**pH**		**(mol/kg)**	**(mol/kg)**	**diff**	(mol alkalinity)	(mol amine)
1	VLE-01	**0.1**	VLE	0.999	51.692	12.100	10.418	9.736	5.26	**5.28**	1.9474	2.79		**0.70**	**0.70**
			40C	0.996	51.581	11.960	10.418	9.736	5.28	0.682	1.9548	2.80	0.2		
											1.9511	2.79	-0.4		
2	VLE-02	**0.1**	VLE	0.998	62.067	21.460	10.418	9.736	5.25	**5.28**	2.0003	2.79		**0.72**	**0.72**
			40C	0.999	62.016	21.372	10.418	9.736	5.26	0.682	2.0001	2.76	0.0		
											2.0002	2.78	1.1		
3	VLE-03	**0.1**	VLE	1.292	61.036	12.748	10.418	9.736	5.25	**5.28**	1.8423	2.80		**0.66**	**0.66**
			40C	1.380	61.150	9.800	10.418	9.736	5.26	0.682	1.8358	2.77	-0.2		
											1.8391	2.79	0.9		
4	VLE-04	**0.1**	VLE	1.200	52.677	14.762	10.418	9.736	5.25	**5.28**	1.5514	2.83		**0.55**	**0.55**
			40C	1.333	52.958	10.928	10.418	9.736	5.26	0.682	1.5509	2.82	0.0		
											1.5512	2.83	0.3		
5	VLE-05	**0.1**	VLE	1.831	56.599	8.548	10.418	9.736	5.25	**5.28**	1.2935	2.86		**0.45**	**0.45**
			40C	1.787	58.472	11.940	10.418	9.736	5.26	0.682	1.2829	2.86	-0.4		
											1.2882	2.86	0.1		
6	VLE-06	**0.1**	VLE	1.576	59.630	12.680	10.418	9.736	5.24	**5.28**	1.4679	2.85		**0.52**	**0.52**
			40C	1.623	60.362	11.796	10.418	9.736	5.26	0.682	1.4752	2.85	0.2		
											1.4715	2.85	-0.1		
7	VLE-07	**0.1**	VLE	1.324	45.470	16.946	10.251	9.690	5.26	**5.3**	1.0560	2.92		**0.36**	**0.36**
			40C	1.310	45.561	17.138	10.251	9.690	5.26	0.561	1.0634	2.92	0.4		
											1.0597	2.92	0.1		
8	VLE-08	**0.1**	VLE	1.440	45.758	20.452	10.251	9.690	5.28	**5.3**	0.8592	2.95		**0.29**	**0.29**
			40C	1.376	45.877	21.728	10.251	9.690	5.28	0.561	0.8571	2.94	-0.1		
											0.8582	2.94	0.4		
9	VLE-09	**0.1**	VLE	1.637	45.804	23.004	10.251	9.690	5.25	**5.3**	0.6793	2.96		**0.23**	**0.23**
			40C	1.574	45.982	23.450	10.251	9.690	5.26	0.561	0.6979	2.96	1.4		

Table C3 Calculations for High Pressure Equipment at 120°C temperature (3M AM)

Sample nr:		VIPPE 01	VIPPE 02	VIPPE 03
Type amin:		3M AMP	3M AMP	3M AMP
Date:	Ddmmåå	30/01/2012	30/01/2012	30/01/2012
W(H20)	G	726.1	726.1	726.1
W(AMP)	G	267.42	267.42	267.42
W(Pz)	G	0	0	0
Concentration:	Vekt %	26.9	26.9	26.9
n(H20)	Mol	40.30	40.30	40.30
n(AMP)	Mol	3.00	3.00	3.00
n(Pz)	Mol	0.00	0.00	0.00
x(H20)	Molfraction	0.9307	0.9307	0.9307
x(AMP)	Molfraction	0.0693	0.0693	0.0693
x(Pz)	Molfraction	0.0000	0.0000	0.0000
C(AMP)	mol/kg	3.02	3.02	3.02
C(Pz)	mol/kg	0.00	0.00	0.00
C(AMP+Pz)	mol/kg	3.02	3.02	3.02
Density (apparent)	mol/cm3	0.9935	0.9935	0.9935
Gas Phase				
Totalpressure	bara	9.512	8.864	7.851
Totalpressure	kPa	951.2	886.4	785.1
Temperature	oC	120.09	119.95	120.04
Temperature	K	393.24	393.10	393.19
P (H2O)	bar	1.8520	1.8439	1.8493
P (amin)	bar	1.7741	1.7663	1.7715
P (CO2)	bar	7.74	7.10	6.08
P (CO2)	kPa	773.79	709.77	607.95
Liquid sample				
Weight empty	g	1652.57	1652.62	1652.66
Weight empty + unloaded	g	1750.52	1766.12	1746.49
weight empty + unloaded + loaded	g	1809.89	1808.49	1808.4
Amine Analysis				
Total weight sample	g	157.32	155.87	155.74
Weight unloaded sample	g	97.95	113.5	93.83
Weight loaded sample	g	59.37	42.37	61.91

Dato:	ddmmåå	30/01/2012	30/01/2012	30/01/2012
Parallell 1:				
Sample weight	g	2.014	2.52	2.492
HCl	g	47.488	47.871	47.144
NaOH	ml	23.2523	26.91	18.2552
pH:		5.25	5.25	5.25
CO2 conc (unloaded + loaded)	mol/kg	0.5921	0.4082	0.5719
CO2 conc (loaded sample)	mol/kg	1.5689	1.5018	1.4386
Parallell 2:				
Sample weight	g	2.1	2.543	2.449
HCl	g=ml	47.777	47.749	47.124
NaOH	g=ml	23.007	26.556	19.4943
pH:		5.25	5.25	5.25
CO2 conc (unloaded + loaded)	mol/kg	0.5806	0.4091	0.5562
CO2 conc (loaded sample)	mol/kg	1.5384	1.5050	1.3992
Blind Sample				
HCl	g=ml	10.257	10.257	10.257
NaOH	g=ml	9.8708	9.8708	9.8708
pH:		5.25	5.25	5.25
Blank Sample	g=ml	0.3862	0.3862	0.3862
Avg CO2 conc (loaded sample)	mol/kg	1.5537	1.5034	1.4189
% difference	%	1.99	-0.21	2.82
Amine concentration A	mol/kg	2.96	2.96	3.00
Amine concentration B	mol/kg	2.99	2.98	3.00
Average Amine Concentration	mol/kg	2.97	2.97	3.00
Amine conc (approx amine conc):	mol/kg	2.8131	2.8198	2.8310
Loading basert på ber. Amin	mol CO2/mol amin	0.5523	0.5331	0.5012
Loading from analysis	mol CO2/ mol Amine	0.5173	0.5065	0.4664